AFRL-HE-WP-TR-2003-0092

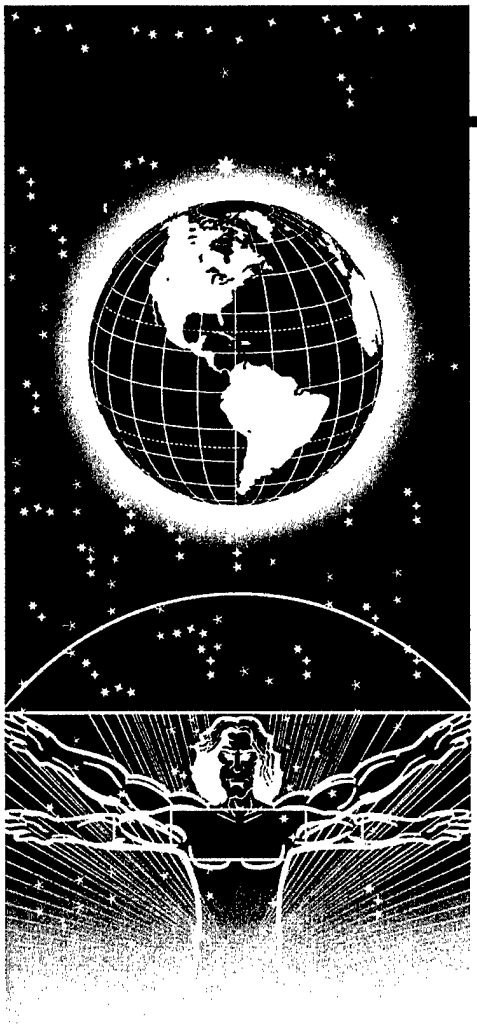

UNITED STATES AIR FORCE RESEARCH LABORATORY

DARPA

RUGGEDIZED, FULL-COLOR, FLEXIBLE OLED DISPLAY

Michael Hack
UNIVERSAL DISPLAY CORPORATION
EWING NJ 08618

Stephen R. Forrest
PRINCETON UNIVERSITY
PRINCETON NJ 08544

Mark Thompson
UNIVERSITY OF SOUTHERN CALIFORNIA
LOS ANGELES CA 90089

Tom Jackson
PENNSYLVANIA STATE UNIVERSITY
UNIVERSITY PARK PA 16802

Robert Praino
VITEX SYSTEMS, INC.
SAN JOSE CA 95134

David Huffman
L3 DISPLAYS
ALPHARETTA GA 30004

JUNE 2003

INTERIM REPORT FOR THE PERIOD 15 JUNE 2000 TO 26 DECEMBER 2002

Human Effectiveness Directorate
Crew System Interface Division
2255 H Street
Wright-Patterson AFB, OH 45433-7022

NOTICES

When US Government drawings, specifications, or other data are used for any purpose other than a definitely related Government procurement operation, the Government thereby incurs no responsibility nor any obligation whatsoever, and the fact that the Government may have formulated, furnished, or in any way supplied the said drawings, specifications, or other data, is not to be regarded by implication or otherwise, as in any manner licensing the holder or any other person or corporation, or conveying any rights or permission to manufacture, use, or sell any patented invention that may in any way be related thereto.

Please do not request copies of this report from the Air Force Research Laboratory. Additional copies may be purchased from:

National Technical Information Service
5285 Port Royal Road
Springfield VA 22161

Federal Government agencies and their contractors registered with the Defense Technical Information Center should direct requests for copies of this report to:

Defense Technical Information Center
8725 John J. Kingman Road, Suite 0944
Ft. Belvoir VA 22060-6218

TECHNICAL REVIEW AND APPROVAL

AFRL-HE-WP-TR-2003-0092

This report has been reviewed by the Office of Public Affairs (PA) and is releasable to the National Technical Information Service (NTIS). At NTIS, it will be available to the general public.

This technical report has been reviewed and is approved for publication.

FOR THE COMMANDER

MARIS M. VIKMANIS
Chief, Crew System Interface Division
Air Force Research Laboratory

REPORT DOCUMENTATION PAGE

Form Approved
OMB No. 0704-0188

1. AGENCY USE ONLY (Leave blank)	2. REPORT DATE	3. REPORT TYPE AND DATES COVERED
	June 2003	INTERIM REPORT 15 June 2000 - 26 December 2002

4. TITLE AND SUBTITLE

RUGGEDIZED, FULL-COLOR, FLEXIBLE OLED DISPLAY

5. FUNDING NUMBERS

C: MDA972-00-C-0017
PE: 62708E
PR: H731
TA: 09
WU: 01
JON: 71841103

6. AUTHOR(S)

(1) Michael Hack, (2) Stephen R. Forrest, (3) Mark Thompson, (4) Tom Jackson, (5) Robert Praino and (6) David Huffman

7. PERFORMING ORGANIZATION NAME(S) AND ADDRESS(ES)

(1) Universal Display Corp. (UDC), 375 Phillips Blvd, Ewing, NJ 08618-1428; (2) Princeton U., Dept. of EE, Princeton NJ 08544; (3) U. of So. Calif., 840 Downey Way, Los Angeles, CA 90089-0744; (4) Penn. St. U., Dept of Elec. Engr, 121 Elec. Engr. East, University Park, PA 16802; (5) Vitex Sys., 3047 Orchard Pkwy, San Jose, CA 95134; (6) L3 Comm. Displays, 1355 Bluegrass Lakes Pkwy, Alpharetta GA 30004

8. PERFORMING ORGANIZATION

9. SPONSORING/MONITORING AGENCY NAME(S) AND ADDRESS(ES)

Air Force Research Laboratory
Human Effectiveness Directorate
Crew System Interface Division
Air Force Materiel Command
Wright-Patterson AFB OH 45433-7022

10. SPONSORING/MONITORING

AFRL-HE-WP-TR-2003-0092

11. SUPPLEMENTARY NOTES

12a. DISTRIBUTION/AVAILABILITY STATEMENT

Approved for public release, distribution is unlimited.

12b. DISTRIBUTION CODE

13. ABSTRACT *(Maximum 200 words)*

The objective of this program was to demonstrate a flexible, rugged, bright and efficient phosphorescent OLED technology with a low cost manufacturing path. The team comprised Universal Display Corporation, Princeton University, the University of Southern California, Penn State University, L3 Displays and Vitex Systems, and was led by Universal Display Corporation (PI: Michael Hack). The program focused on developing the technology to enable reliable low power consumption flexible (FOLED™) displays to be fabricated on plastic substrates. This involved the integration of phosphorescent OLEDs (PHOLED™s) with multi-layer permeation barriers deposited over the substrate and also as a thin film encapsulant over the OLED to prevent degradation by oxygen or moisture. Additional tasks were development of large area, low cost organic vapor phase deposition (OVPD™) fabrication technology, along with novel approaches to demonstrating bistable OLED pixels for advanced displays with reduced information bandwidth requirements. Accomplishments included the demonstration of thin film encapsulated OLED pixels on plastic substrates with lifetimes exceeding 2,000 hours, the delivery to the government of monochrome, phosphorescent OLED passive-matrix displays on plastic substrates, high performance OLEDs and TFTs grown using OVPD, and bistable OLED pixels fabricated from both a novel integrated organic OLED (TOLED™) integrated with an organic photodetector, as well as a second approach utilizing OLEDs and amorphous silicon TFTs.

14. SUBJECT TERMS
Flexible displays, organic light emitting devices (OLED) and materials, organic vapor phase vacuum deposition (OVPD), phosphorescent OLED (PHOLED), transparent OLED (TOLED), encapsulation, barrier coated substrates, thin-film transistor (TFT), bistable pixels

15. NUMBER OF PAGES
68

16. PRICE CODE

17. SECURITY CLASSIFICATION OF REPORT	18. SECURITY CLASSIFICATION OF THIS PAGE	19. SECURITY CLASSIFICATION OF ABSTRACT	20. LIMITATION OF ABSTRACT
Unclassified	Unclassified	Unclassified	Unlimited

NSN 7540-01-280-5500

Standard Form 298 (Rev 2-89) Prescribed by ANSI Std Z-39-18
298-102 COMPUTER GENERATED

This page intentionally left blank.

CONTENTS

LIST OF FIGURE CAPTIONS

LIST OF TABLE TITLES

FOREWORD

This contract MDA972-00-C-0017 to Universal Display Corp. was effective on 15 June 2000. The contract title was "Ruggedized, Full-color, Flexible OLED Display." The original contract statement of work covered 18 months for two tasks: Task 1, the demonstration of flexible displays and Task 2, the development and characterization of rugged packaging for flexible displays. Task 3, the development of large area, low cost, OVPD flexible display fabrication technology, was an option to the original contract; this Task 3 was funded on 9 January 2001. During 2002 two additional tasks were added, both with a period of performance from 26 June 2001 to 25 June 2002. Task 4 was added to develop integrated monolithic encapsulation at Vitex Inc. in San Jose CA. Task 5, was added to create and demonstration bistable pixels at Princeton and Pennsylvania State Universities. The period of performance for the contract was subsequently extended (at no cost to the government) until 26 December 2002.

Funding for all Tasks 1-4 was a 50:50 cost share between the government and the contractor Task 5 was $677,471 with $450,000 from the government and $227,471 cost share from the contractor.

Total program: $2,977,471 ($1,600,000 DARPA, $1,377,471 contractor)
Tasks 1 and 2: $1,200,000; Task 3: $500,000; Task 4: $600,000; Task 5: $677,471
ARPA Orders (AO): $500K in FY00 under AO H731/09 (FY00,62708E/0T10);
$1100K in FY01 (two AO's for $250K and $850K) (FY01, 62708E/1T10)

In addition to this report, the results of this project are documented in 31 publications listed in Appendix A. Graduate degrees awarded with funding under this effort are listed in Appendix B. Two patent applications have been made and when issued will be available at the Patent Office.

This report has been formatted in accordance with a commercial standard, with tailoring from the AFRL Scientific Technical Information Office. That standard is:
"Scientific and Technical Reports—Elements, Organization, and Design,"
American National Standard ANSI/NISO Z39.18-1995 (NISO Press, Bethesda MD, 1995),
which is available electronically via the following website address:
http://www.wrs.afrl.af.mil/library/sti-pubh.htm

The technical review of this document was accomplished by Dr. Darrel G. Hopper of AFRL.

PREFACE

The objective of this applied research program was to develop flexible, rugged, bright and efficient small molecule organic light-emitting diode (OLED) technology with a low cost manufacturing path. This contract enabled the Team to leverage technology arising from an earlier DARPA grant F33615-94-1-1414, awarded to Princeton University in 1994, which in turn built from basic research results on materials funded in the early 1990s by the Air Force Office of Scientific Research and the Office of Naval Research.

Universal Display Corporation assembled a team comprising the Princeton University, the University of Southern California, Vitex Corporation, L3 Communications Displays, and the Pennsylvania State University. Universal Display Corporation concentrated on integrating the various OLED display technologies, display design, process development and display fabrication, along with device characterization and lifetime studies. The Princeton University and the University of Southern California developed ultra-high efficiency OLEDs. The Princeton University was also responsible for the scale-up of the innovative organic vapor phase deposition (OVPD) and the demonstration of a bistable OLED pixel utilizing only organic active components. Vitex, Inc. developed low permeation barrier coated plastic substrates in addition to monolithic thin film encapsulation. The Pennsylvania State University accomplished the development and fabrication of a hybrid amorphous silicon/OLED bistable pixel array, and L3 Communications Displays performed characterization and environmental testing of UDC's prototype displays.

The DARPA-funded AFRL-managed research and development effort reported here has now been transitioned to the Army Research Laboratory (ARL). Two ARL cooperative agreements were awarded in 2002, one to UDC (DAAD19-02-2-0019) and one to the Princeton University (DAAD19-02-2-0018). Each effort involves a teaming arrangement similar to this now completed effort.

ACKNOWLEDGEMENTS

We gratefully acknowledge the financial support received from DARPA under Contract Number MDA972-00-C-0017 under the DARPA High Definition Systems Flexible Displays program managed by Drs. Bruce Gnade and Robert Tulis. We especially thank Dr. Darrel G. Hopper of AFRL for his support throughout the project as the DARPA Agent and Contracting Officer's Technical Representative (COTR).

This page intentionally left blank.

1. SUMMARY

The objective of this program was to develop and deliver flexible, rugged, bright and efficient small molecule organic light-emitting diode (OLED) technology with a low cost manufacturing path. OLEDs are particularly well suited for use in flexible displays due the flexibility of the thin films of which they are comprised. Plastics are an attractive candidate for the flexible substrate because of their manufacturability and cost-effectiveness. The principal limitation of OLED displays on plastic, however, is their lifetime. The materials currently used in OLEDs are very sensitive to moisture and oxygen, and plastic substrates are generally too highly permeable to both to be suitable for OLEDs. Development of a long-lived flexible OLED (FOLED) display on plastic therefore poses two major challenges: preventing moisture and oxygen diffusion into the display area from the bottom/substrate and also from the top, through a thin film encapsulation deposited onto the OLED devices. Our approach to solving this problem was to employ a multilayer barrier stack on the substrate as well as the OLED.

A second part of the program was to develop a new low cost manufacturing solution for OLED devices. This was based on Organic Vapor Phase Deposition (OVPD) which allows for rapid deposition of small molecular weight organic thin films on continuous flexible backplanes, with a very high material utilization. The final task was the development of bistable OLED pixels for future flat panel displays that both minimize power consumption and reduce display information bandwidth requirements. This can be achieved by fabricating bistable pixels, which only need to be addressed when their state is to be changed i.e. from on to off.

Major achievements accomplished during this project are listed below.

- Demonstrated a new high efficiency red phosphorescent device at CIE = (0.65, 0.35) with a luminous efficiency of 12 cd/A and a lifetime to half-brightness of >15,000 hours for an initial luminance of 300 cd/m^2

- Demonstrated a new high efficiency green phosphorescent device at CIE = (0.31, 0.64) with a luminous efficiency of 24 cd/A and a lifetime to half-brightness of >13,000 hours for an initial luminance of 600 cd/m^2

- Significantly improved the lifetime of thin film encapsulated OLEDs on barrier coated plastic substrates to > 2,000 hours (extrapolated)

- Significantly improved the lifetime of thin film encapsulated OLEDs on barrier coated glass substrates to > 3,000 hours (extrapolated)

- Delivered to the government monochrome, video-rate phosphorescent OLED passive-matrix displays on plastic substrates

- Developed a new custom tool at Vitex facility for the encapsulation of OLED displays

- Fabricated an integrated organic transparent OLED/organic photodetector and demonstrated an organic bistable pixel

- Fabricated working arrays of bistable pixels containing OLEDs and amorphous silicon devices

- Grown high performance organic TFTs and PHOLEDs using Organic Vapor Phase Deposition

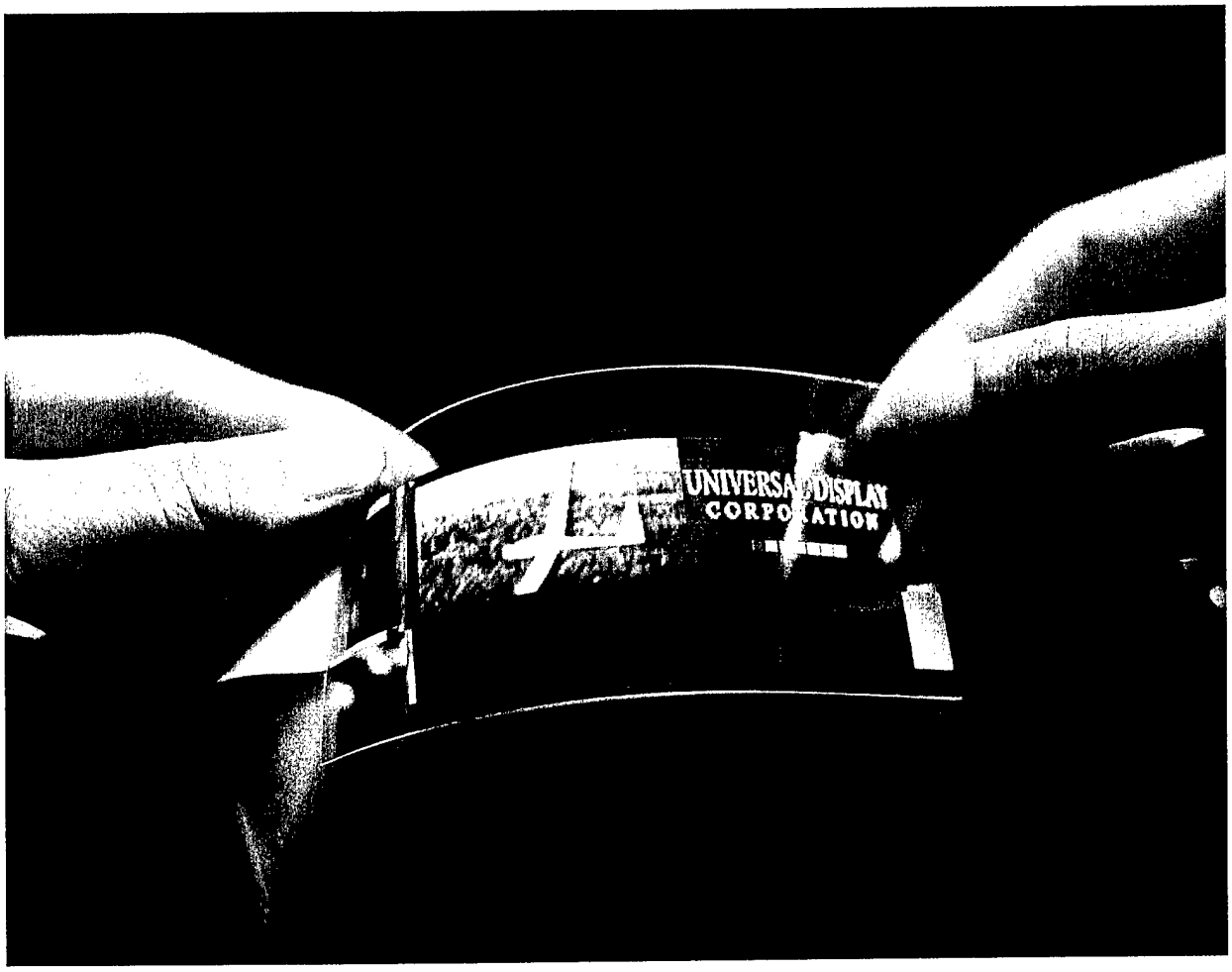

Figure 1: A 240 column by 64 row passive matrix video rate display fabricated on a plastic substrate (UDC, June 2001)

2. INTRODUCTION

A conventional OLED structure based on small molecular weight compounds is shown schematically in Figure 2. Briefly, the device is structured as follows: On top of a glass substrate, typically equal to or less than 1 mm in thickness, is grown a transparent conducting anode using such materials as indium tin oxide (ITO). This anode is often deposited by sputtering in vacuum prior to the deposition of the organic layers. Next, a material that preferentially conducts holes, or the hole transporting layer (HTL) is deposited by vacuum thermal evaporation in a chamber whose background pressure is $<10^{-6}$ Torr to a thickness of approximately 50 nm. Next follows the deposition of an equal thickness of an electron transporting layer (ETL). In the original OLEDs demonstrated in 1985, the ETL material also emitted green light, making the ETL serve the dual purpose of transporting electrons as well as providing the light emission. The device is then completed by deposition of a low work function metal cathode providing efficient electron injection into the ETL. Metal such as mixtures of Mg and Ag, or LiF and Al are most frequently used for this purpose.

In operation, the cathode is connected to the negative terminal of a power supply, and the anode is grounded. Then, electrons and holes are injected from the cathode and anode contacts, respectively, and are transported by the ETL and HTL to the interface between these two layers. At this point, the electron and hole form a coulombically bound state on a molecule in the ETL. This state, which can also be considered a molecular excited state, called an exciton, can diffuse through the ETL until the electron and hole recombine. The energy lost in that recombination process generates either heat (if the recombination is via a defect), or light. The light is then emitted and those photons which emerge within the critical angle of the glass/air interface are then emitted and are seen by the observer. An OLED such as that in Figure 2 typically has an external quantum efficiency (i.e. the ratio of electrons injected to the number of photons observed) of ~1%, and an operational lifetime of ~1,000 hrs.

The device can be made much more efficient by "doping" either the HTL or ETL with a highly luminescent molecule, whose energy of luminescence is lower than that of the host HTL or ETL material (i.e. it is red shifted in color). Then, as excitons are formed in the host at the HTL/ETL interface, it becomes energetically favorable for the excited state to transfer from the host to the luminescent molecule. Because the luminescent molecule (also known as the lumophore) is only at low concentrations (1%-10%) within the host, they are isolated from each other. Hence, the exciton cannot easily diffuse around the material layer where it might encounter a non-radiative defect site. In this case, the quantum efficiency of the device can be greatly improved. Indeed, using phosphorescent dopants, along with "blocking layers" that energetically confine the excitons and charge carriers within the luminescent zone of the OLED, we have observed ~20% external quantum efficiency, corresponding to ~100% internal efficiency for phosphorescent OLEDs. Here, blocking layers are such that they have energy gaps larger than that of the luminescent layer such that molecular excited states need to gain energy to hop to molecules within the blocking layer. The blocking layer thickness is generally kept thin (~10 nm or less) to avoid increasing the operating voltage of the OLED. Indeed, by keeping the entire thickness of the resistive organic layers to ~100 nm, the operating voltage is typically ~6V.

Finally, the doping of the emission zone also increases the operational lifetime of the OLED. Typical operating lifetimes are in the range of 50,000 – 100,000 hours for the doped red and green PHOLEDs demonstrated in this program (conditions: room temperature and display luminance of about 100 cd/m^2). Here, lifetime is defined as the time for the luminance to decrease to half of its initial value.

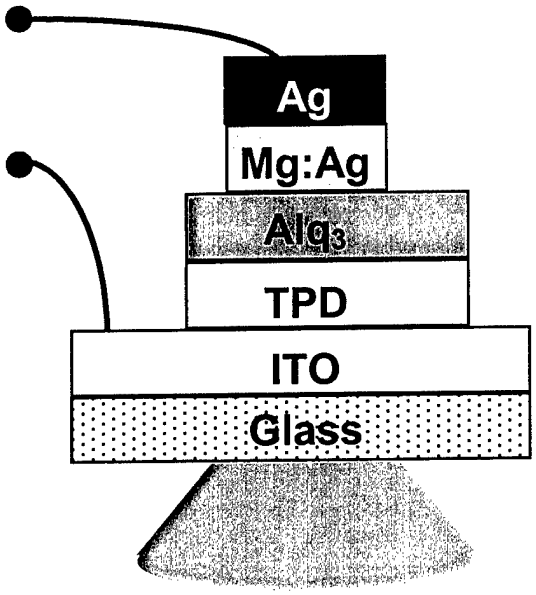

Figure 2: Schematic diagram of a simple fluorescent organic light emitting device. Here, Alq_3 is an electron transporting and green emissive material, and N,N-di-(3-methylphenyl)-N,N diphenyl-4,4-diaminobiphenyl (TPD) is a hole transport material.

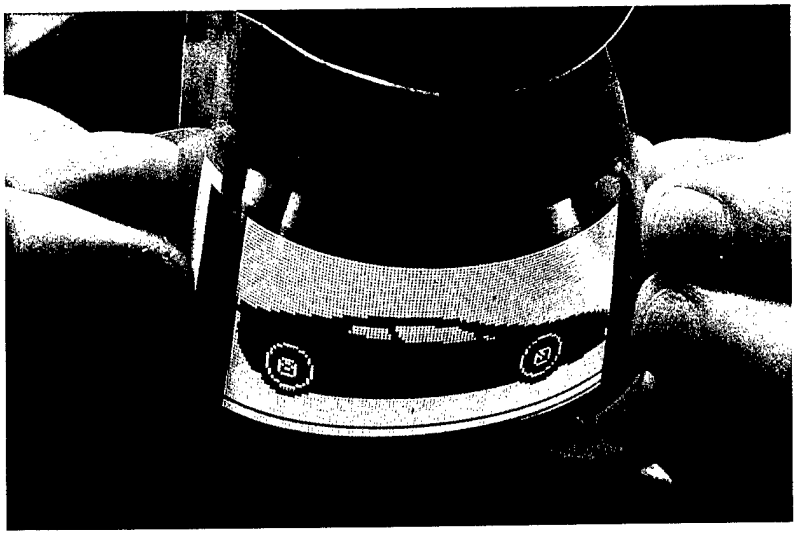

Figure 3: World's first functional unencapsulated passive matrix OLED Display.Demonstrated in 2000 by UDC based on work accomplished by UDC, PU, and USC (May 2000)

In 2000 UDC demonstrated a passive matrix OLED display, as shown in Figure 3. This flexible monochrome passive matrix display had 128 columns and 64 rows with a 400um by 500um pixel pitch. The key goal of this program was to develop the encapsulation technology necessary to enable this type of FOLED to live for as long as similar displays fabricated on glass substrates, and employing glass or metal lid packages.

The Program consisted of five Tasks, the first three from the original grant in 2000 with a period of performance of 7/1/00 to 6/26/02, and Tasks 4 and 5 which were added in 2001 with a period of performance from 7/1/01 until 12/26/02. In summary the Tasks were:

Task 1:
Demonstrate flexible displays and optimize display drive architectures.

Task 2:
Develop and characterize rugged packaging for flexible displays

Task 3:
Develop large area, low cost, organic vapor phase deposition (OVPD) flexible display fabrication technology.

Task 4:
Develop integrated thin film encapsulation at Vitex's San Jose facility.

Task 5:
Demonstrate bistable OLED pixels:
a) All organic bistable smart pixel
b) Hybrid bistable OLED pixel using amorphous Si TFTs

3. METHODOLOGY AND RESULTS

We now discuss in detail some of the highlights of the accomplishments of our team.

3.1 Flexible, long-lived, low power consumption OLED Displays

The overall mission of the program was to develop and deliver flexible, rugged, bright and efficient small molecule organic light-emitting diode (OLED) technology with a low cost manufacturing path. OLEDs are particularly well suited for use in flexible displays due the flexibility of the thin films of which they are comprised. Plastics are an attractive candidate for the flexible substrate because of their manufacturability and cost-effectiveness. The principal limitation of OLED displays on plastic, however, is their lifetime. The materials currently used in OLEDs are very sensitive to moisture and oxygen, and plastic substrates are generally too highly permeable to both to be suitable for OLEDs. Development of a long-lived flexible OLED (FOLED) display on plastic therefore poses two major challenges: preventing moisture and oxygen diffusion into the display area from the bottom/substrate and also from the top. As outlined in the Statement of Work, our approach to solving this problem was to employ a multilayer barrier stack on the substrate as well as the OLED (see Figure 4). The barrier coatings on the substrate and display are comprised of alternating layers of inorganic oxide and polyacrylate. The inorganic oxide layers act as diffusion barriers to water/oxygen while the polymer layers decouple defects in the oxide as well as allow for greater flexibility in an otherwise rigid coating.

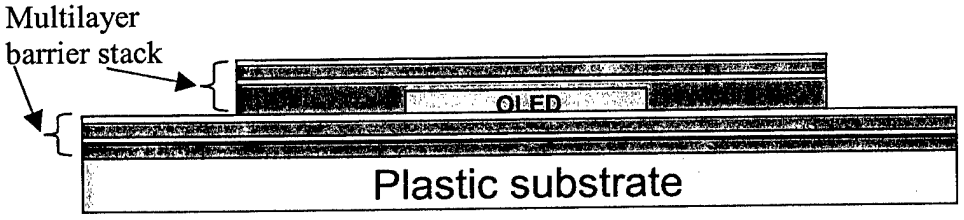

Figure 4: Schematic diagram of multilayer barrier stack coatings on both a plastic substrate as well as an OLED that is built on the barrier coated plastic substrate.

Our achievements and progress towards this goal are described below, followed by a summary of completed deliverables.

3.1.1 Demonstration of Highly Efficient and Stable Phosphorescent OLED Technology

During the course of the program, the efficiencies, color tunability, and lifetimes of UDC phosphorescent OLEDs (PHOLEDs) improved significantly. Of particular note was the achievement of excellent lifetimes for both the red and green PHOLED devices, and a relatively saturated blue with CIE = (0.14, 0.23). Table I shows the current status of UDC PHOLEDs. For each color, the table lists the CIE coordinates based on the electroluminescent spectrum at 10 mA/cm^2, luminance and luminous efficiency at 1 mA/cm^2, and half life at the indicated starting luminance.

Table I: December 2002 status of a sub-set of UDC PHOLEDs.

Color	Red	Orange -Red	Green	Light Blue	Deep Blue
CIE (x, y)	*0.65, 0.35*	*0.61, 0.38*	*0.30, 0.65*	*0.14, 0.37*	*0.14, 0.23*
Luminous Efficiency (cd/A) at 1 mA/cm^2	*12*	*22*	*24*	*16*	*10*
Luminance (cd/m^2) at 1 mA/cm^2	*120*	*220*	*240*	*160*	*100*
Lifetime (hours)	*15,000 @ 300 cd/m^2*	*> 15,000 @ 300 cd/m^2*	*13,000 @ 600 cd/m^2*	Under development	Under development

3.1.2 Flexible Substrate Characterization

One of the first tasks of the program was to characterize the barrier coated PET substrates that would eventually be used towards the final delivery of an encapsulated phosphorescent OLED (PHOLED) display on plastic. To quantify the moisture permeation rate of the barrier substrate beyond the $5x10^{-3}$ g/m^2/day limit of MOCON[1] detection instruments, a 50 nm thick layer of Ca was deposited on top of the barrier using thermal evaporation. A 1 μm thick protection layer of Cu was subsequently deposited onto the calcium without breaking vacuum and a glass substrate was adhered to the entire substrate using an epoxy face seal so that the sole route for moisture ingress to the Ca layer was through the substrate. The calcium was optically monitored for the formation of transparent calcium hydroxide caused by water or oxygen permeation (Figure 5). Measurements on substrates with five alternating polyacyrlate/Al_2O_3 layers after 1,632 hours of exposure to atmosphere at room temperature yielded an area of reacted Ca equal to 0.74% of the total area. Assuming that the transparent regions were fully reacted, and using a calcium density of 1.55 g/cm^3 and a molar mass of 40.1, the permeation rate was estimated to be $4x10^{-6}$ g/m^2/day. The localized nature of the corroded areas suggests that permeation was dominated by pinhole defects rather than bulk permeation.

PHOLED test pixels (5 mm^2) were then fabricated on 178 μm thick PET substrates coated with an organic-inorganic multilayer barrier film (FG500, see Figure 6) and their rates of degradation were compared to that of glass-based devices. Figure 7 shows a typical plot of normalized luminance vs. time for an $Ir(ppy)_3$ based PHOLED on FG500. The PHOLED was grown via conventional vacuum thermal evaporation by sequentially depositing layers of copper phthalocyanine (CuPc) [10 nm], 4,4'-bis[N-(1-napthyl)-N-phenyl-amino] biphenyl (α-NPD) [30 nm], 4,4'N,N'-dicarbazole-biphenyl (CBP) [30 nm] doped with an electrophosphorescent dopant *fac* tris(2-phenylpyridine)iridium ($Ir(ppy)_3$) at a concentration of 6% by weight, aluminum(III)bis(2-methyl-8-quinolinato)4-phenylphenolate (BAlq) [10 nm] and tris-(8-hydroxyquinoline) aluminum (Alq_3) [40 nm], using a 1 nm layer of lithium fluoride (LiF) and a 100 nm layer of aluminum as the cathode contact. The PHOLED was then encapsulated in a dry nitrogen atmosphere (<1 ppm H_2O) using a glass lid and UV cured epoxy edge seal. A CaO getter was added inside the package to react with any byproducts of the epoxy cure and any residual water or oxygen present within the encapsulated volume. The encapsulation for the glass based PHOLED was the same as that for the PHOLED on FG500, including the CaO getter.

[1] MOCON 3/31G, Minneapolis, MN 55428.

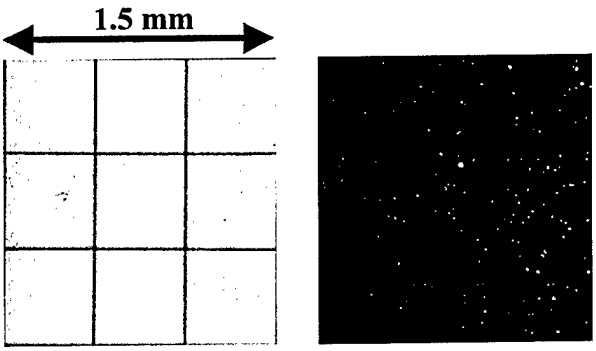

Figure 5: Determination of moisture permeation rate using the Ca test. These images show a 2.25 mm^2 area of a 50 nm thick layer of calcium deposited onto barrier coated PET viewed through the substrate: (a) Image after 1,632 hours of exposure to atmosphere; (b) Simple image analysis of the Ca corrosion sample whereby the grayscale of Ca degradation is processed to yield a two color image with oxidized Ca shown as white against a black background of metallic Ca.

Lifetime of the encapsulated PHOLED on FG500 was measured at an initial luminance of 425 cd/m^2 and a dc constant current drive of 2.5 mA/cm^2 in air with a temperature range of 20-25 °C over the period of measurement. The glass based PHOLED was driven at 2.6 mA/cm^2 (600 cd/m^2). No 'burn in' of either pixel was performed before life testing was started. Time to half luminance of the PHOLED on FG500 was 3,800 hours, as compared to >10,000 hours for the equivalent device made on glass.

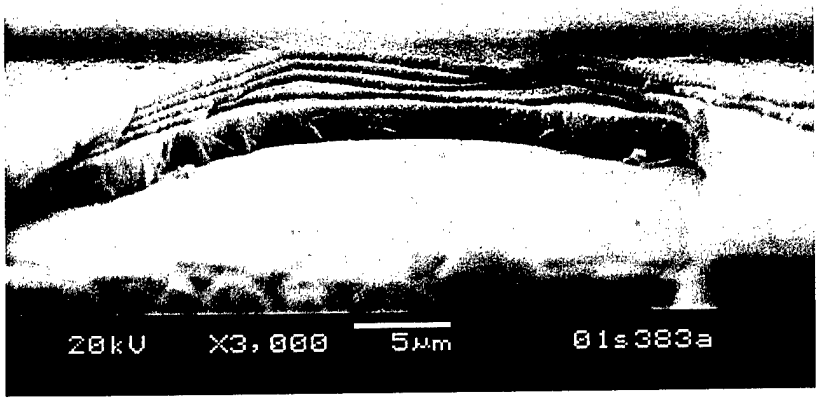

Figure 6: Scanning electron micrograph image of a barrier film cross section.

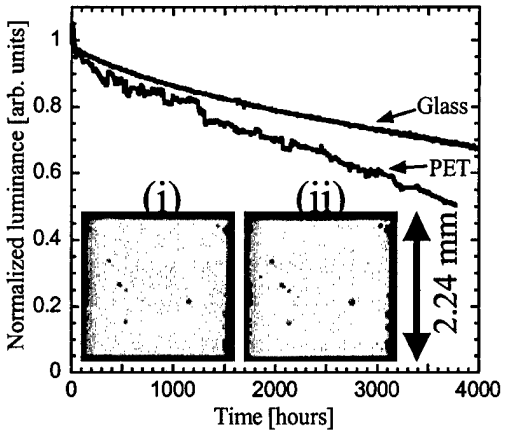

Figure 7: Lifetime plot of an $Ir(ppy)_3$ doped green PHOLED on a barrier coated PET substrate driven at 2.5 mA/cm^2. A PHOLED with the same architecture grown on ITO coated glass is also shown for comparison driven at 2.6 mA/cm^2. The inset figures are images of the FOLED pixel at (i) 1,200 hours and (ii) 3,000 hours. The pixel area is 5 mm^2.

3.1.3 Flexible Display Design

In April-June 2001, UDC designed a 64X240 passive matrix display with 317 μm pixel pitch, and 32 gray levels; this design is illustrated in Figure 8(a). The refresh rate was designed as 120 Hz, and a 64x128 section of the display shows full motion video from a RS-170 or RS-170A source. One important aspect of the electronics design was the incorporation of anti-ghosting electronics. In passive matrix OLED displays, the lack of isolation of each OLED pixel from the array allows for stray charge which can cause ghosting artifacts in the display image, especially if any of the devices have poor diode reverse current-voltage characteristics. To remove these artifacts, the complete array is discharged before every scan line is selected. Fresh data is then applied to the display columns. The electronics also incorporate gray scale correction and are designed to operate using eight (8) AA lithium batteries.

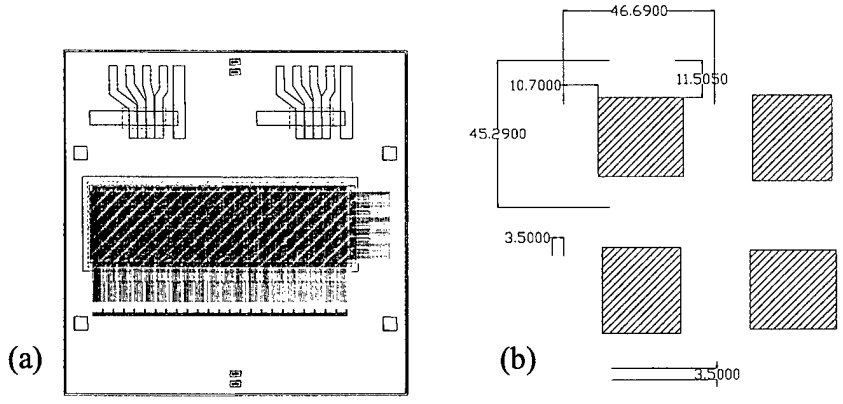

Figure 8: (a) Design layout of the PM3 (one 64 x 240 display with two sets of test pixels); (b) mini-PM3 (four 64 x 64 displays).

To increase throughput and efficiency of data acquisition from the flexible OLEDs (FOLEDs), a modified display was designed at UDC in 2002Q1 (Figure 8(b)). The new display has the same resolution (317 μm pitch) as the FOLED displays delivered throughout this program, but has 64 rows and 64 columns instead of 64 rows x 240 columns. The new design allows four 64x64 displays to be processed on one 4"x4" FG500 substrate as opposed to just one 64x240 display, increasing the development rate of FOLED displays and FOLED display encapsulation.

3.1.4 Flexible Display Yield

During the course of this program, yield of passive matrix displays on flexible substrates was increased considerably. Substantial effort was put forth in 2002Q2 to increase yield through process optimization in conjunction with statistical defect analysis. From our defect analysis, we determined which processing steps were mostly likely to cause the most frequently observed defects and then made the appropriate changes to increase yield. Key modifications included changes to common processing steps which worked well on glass substrates but not on the more vulnerable plastic substrates, for example, baking and solvent rinsing. The modifications improved the plastic processibility. As a result of our efforts, yield of our passive matrix, 317μm pitch displays is >80%. Yield is defined as the number of unencapsulated displays with >95% defect-free pixels divided by the total number of displays. Figure 9 shows typical 64X240 displays before and after the process yield campaign.

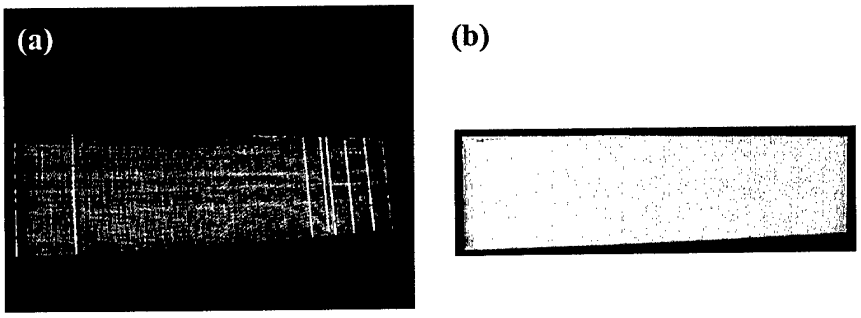

Figure 9: Typical displays fabricated on FG500 (a) before and (b) after the process yield campaign in 2002Q2.

3.1.5 Pixel Encapsulation

In order to provide a rugged, flexible packaging solution to long-lived FOLEDs on plastic, a multilayer, thin film barrier coating was developed to prevent moisture and oxygen diffusion into the display area from the top (see Figure 4). Before attempting to thin film encapsulate PHOLEDs on plastic, however, the encapsulation process was first verified on glass based PHOLEDs. PHOLEDs fabricated on glass substrates were shipped to Battelle's PNNL facility four times during 2000Q4-2001Q4 for monolithic encapsulation experiments. The experiments were generally compromised by the sample transfer in air from the shipping container to the Battelle coating machine which resulted in undesired exposure of the PHOLEDs to moisture, oxygen, and particulates. Nevertheless, some meaningful results were obtained. In the 2001Q4 set of glass based experiments, three out of every four samples were coated with Barix^{TM} 500

film comprising five repeat organic-inorganic layers (see Figure 10). The remaining samples were witnesses to the process in order to separate lifetime problems associated with shipping and handling from those associated with the encapsulation process and/or exposure to air. The witness samples were shipped to Battelle with the samples for monolithic encapsulation. After return shipment to UDC, the witness samples were encapsulated with a glass lid using an epoxy perimeter seal. All samples were subsequently characterized. Although dark spots were observed on every OLED upon initial characterization, the encapsulated OLEDs showed significant improved lifetime over that from similar previous experiments. Figure 11 shows the normalized luminance of a witness sample and a monolithically encapsulated OLED from these experiments. Included for comparison are lifetime data for a standard glass-to-glass PHOLED (glass-based substrate with glass lid and desiccant). All devices are green PHOLEDs driven at constant current density with a starting luminance of 600 cd/m^2.

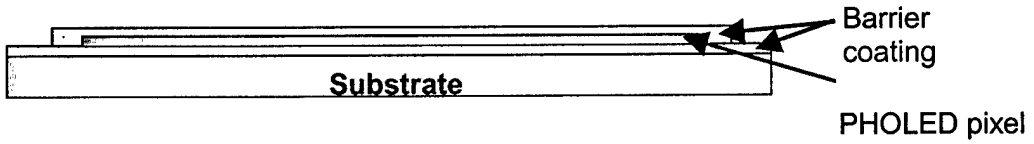

Figure 10: Schematic diagram of a monolithically encapsulated PHOLED pixel.

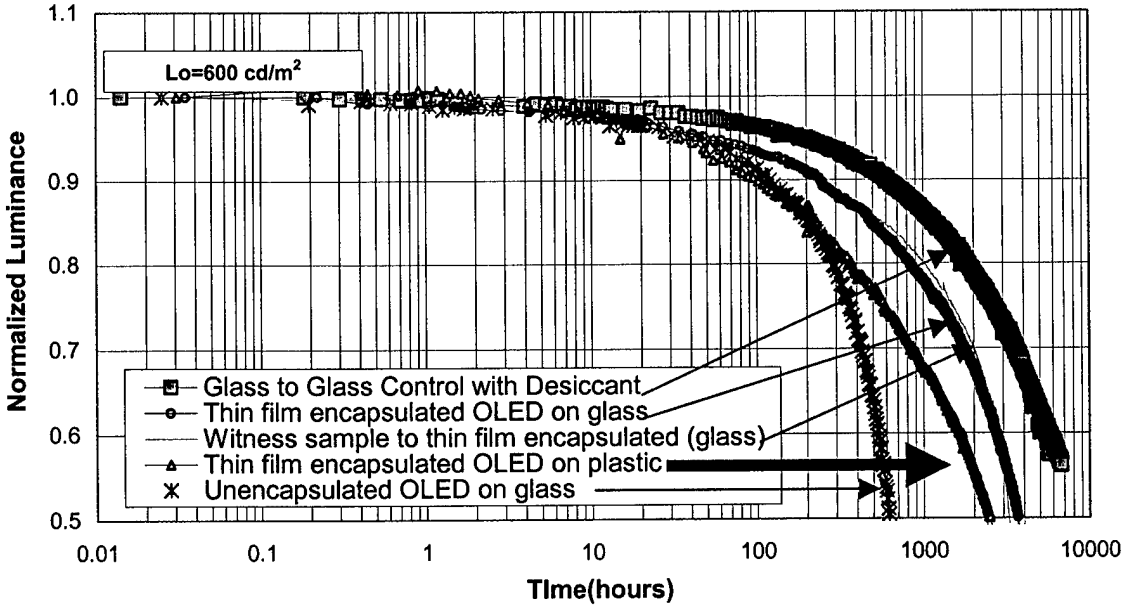

Figure 11: Lifetime data for a thin film encapsulated PHOLED test pixel on glass (circles), unencapsulated (asterisks), witness sample (line), thin film encapsulated PHOLED on plastic (triangles), and glass-to-glass PHOLED packaged with desiccant (squares).

Transfer of the encapsulation process to the Vitex Guardian™ tool, which is integrated with a nitrogen dry box and installed in a class 10,000 clean room at the Vitex laboratory in San Jose, CA, was initiated in 2002Q1. During that time, UDC and Vitex worked together to bring the Vitex Guardian™ tool online for plastic specific processing. Thermal load reduction was identified as a key component in plastic specific process improvement. Various types of substrate fixtures were designed and fabricated to improve PET backside cooling. These resulted in reduced thermal damage to the plastic substrates and improvement in deposition efficiency. Total UV curing power during polymerization of the organic layers in the barrier stack was also identified as an important parameter. Previous work done to explore process windows had shown that UV power level could be reduced within certain limits without impacting the performance of the barrier. UV power was therefore reduced, resulting in significantly improved FOLED performance.

In order to determine if a good barrier could be deposited using the Guardian tool, a multi-layer barrier film stack was deposited on bare PET (Mitsubishi) and sent to Pacific Northwest Labs for calcium permeation testing. The test sample with a calcium film was aged at ambient for 72 hrs as a monitor for any early failures. No degradation of the calcium film was observed. The sample was then placed in an 85°C, 50% RH oven for accelerated testing. There were still no defects after 24 hrs. The overall performance of the Barix stack on PET was sufficient to pass the standard Flexible Glass 500 substrate QC test.

During 2002Q2, UDC and Vitex focused on improving the stability of monolithically encapsulated FOLED test pixels. Figure 11 shows lifetime data of our most reliable monolithically encapsulated FOLED test pixel to date. The 2,500 hour lifetime of the monolithically encapsulated FOLED represents a significant accomplishment; the half life is almost as long as that of the monolithically encapsulated glass-based OLED (3,700 hours).

3.1.6 Display Encapsulation

While we were in the process of developing a thin film encapsulation process under this program, our first approach to encapsulating flexible displays was to seal a foil lid with a desiccant over the plastic substrate. Two such displays were delivered to DARPA during 2001Q3, one to Dr. Bob Tulis/DARPA on August 10th and one to Dr. Darrel Hopper/WPAFB on October 10th. For these deliverables we used technology that was independently reduced to practice outside this program[2,3] to enable the display deliverables until a Vitex solution was available. A schematic diagram of a "lid" package is shown in Figure 12. The package includes a barrier coated plastic lid on which a moisture getter is deposited. The lid is sealed onto the FOLED display using a non-rigid, UV cured adhesive. A second adhesive (Kapton tape, not shown) is applied around the perimeter of the package for additional protection.

---

[2] Silvernail, J. A; Weaver, M. S.; Rothman; M. A. , U.S. Patent No. 6,537,688 B2, Issued 3/25/2003 for ADHESIVE SEALED ORGANIC OPTOELECTRONIC STRUCTURES: Assignee: Universal Display Corporation.

[3] Silvernail, J.; Weaver, M.; Chwang, A. ENCAPSULATION OF AN OLED DISPLAY USING LAMINATION, US Docket # 10/122,969 Filed 4/12/2002

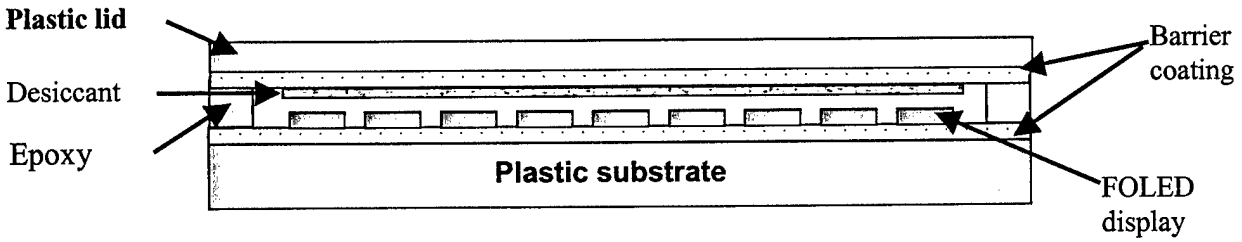

Figure 12: Schematic diagram of a plastic-to-plastic packaged FOLED display

In preparation for thin film encapsulation of passive matrix FOLED displays, test samples with 4 and 6 μm ISM (integrated shadow mask, or cathode separator) structures provided by UDC were coated with a polymer smoothing layer in 2002Q1 (Figure 13). One of the samples was sent to PNNL for a typical flexible barrier substrate Ca test at 85 °C/50% RH. The sample was aged for 144 hrs at ambient to check for any early failure and then placed in the 85 °C/50% RH oven. A few small defects appeared after 96 hrs at 85/50, possibly due to handling or particles. Figures 14 and 15 show the Ca film after 96 and 216 hrs at 85/50, respectively. The overall performance of the barrier over this severe topography is very good and comparable to the performance of a standard Flexible Glass 500 substrate. Flexible Glass has previously been shown to have a WVTR value of less than $8x10^{-5}$ g/m^2-day at ambient conditions in an externally validated, quantitative Ca test.

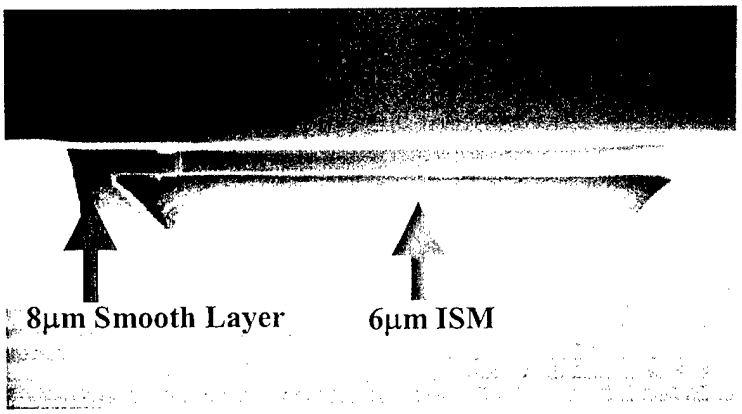

Figure 13: Cross-sectional SEM picture shows an 8 μm thick polymer smoothing layer over a 6μm ISM structure.

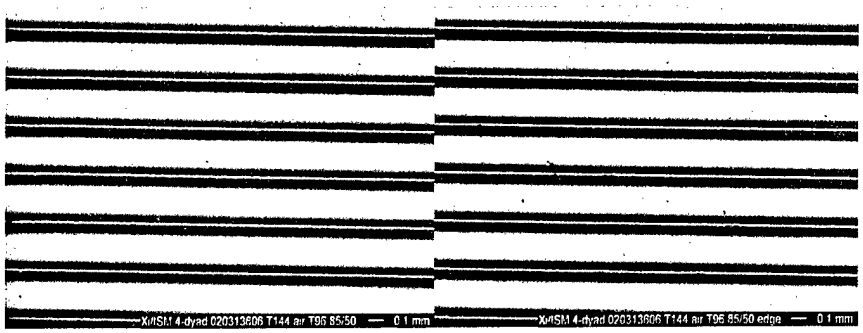

Figure 14: Ca film test at 96 hours of thin film permeation barrier over a 6μm ISM structure.

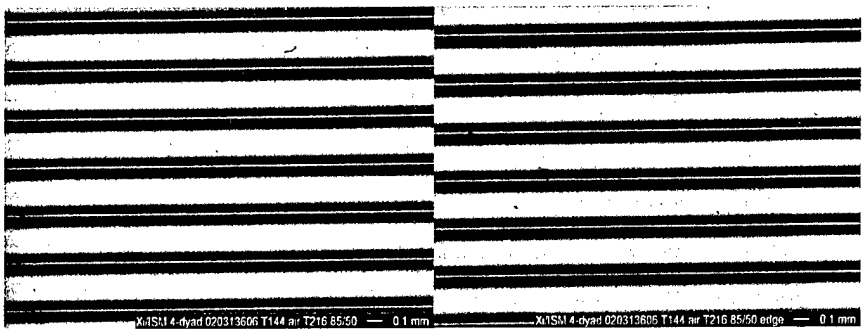

Figure 15. Ca film test at 216 hours of thin film permeation barrier over a 6 μm ISM structure

While the coating experiments with ISM test structures showed that planarization of plastic displays with up to 6 μm step topology could be achieved with the Guardian tool, thin film encapsulation attempts of 317μm FOLED displays during 2002Q2-Q3 resulted in severe damage to the displays. Significant shorting of pixels and rows was evident when the displays were tested. Preliminary experiments indicated that most of the damage occurred upon deposition of the polymer smoothing layer, although a small amount of shorting also occurred with the oxide seed layer. A more extensive failure analysis was carried out during 2002Q3. The experiments were designed to determine the impact of each step in the encapsulation process on the display. The baseline thin film encapsulation for the experiments, in order of deposition on top of the FOLED display, was comprised of 600 Å oxide + 4 um polymer + 600 Å oxide + (0.25 um polymer + 600 Å oxide)x3. The results confirmed that the majority of the damage occurs during the deposition/curing of the first polymer layer. However, a thicker first oxide film better protects the display from damage associated with the polymer layer. Possible explanations for the polymer related damage include stress caused by shrinkage of the polymer as it is curing; bulk change in volume after the polymer cures is approximately 7% according to Vitex. Harmful chemical interactions between the monomer and the OLED materials may also play a role, although the fact that results were similar in tests where the polymer was either deposited on top of a first oxide layer or directly on the display itself suggest that harmful chemical interactions may not play a crucial role. Thermal damage is also a possibility, although temperature sensitive

tape placed on control pieces of plastic during the tests indicate that the temperature does not rise above 40 °C during the monomer deposition or UV curing cycles. We would expect to see thermal related damage only at temperatures above approximately 80 °C. Moreover, exposure to UV alone, which is potentially a heat inducing process, did not result in any damage to the display. Further experiments in 2002Q4 suggested that the polymer related damage is due to shrinkage. Glass based displays were also encapsulated in 2002Q4; the results indicated that the shoring related damage is not particular to the plastic based displays.

3.1.7 Flexibility Testing

Throughout the program, flex test results were obtained for OLED test pixels on plastic (2001Q1), patterned display substrates on plastic (2001Q2 and 2001Q3), and barrier coated plastic substrates (2001Q4). The tests initially involved wrapping the samples around cylinders of various diameters. Experiments performed on 5 mm^2 OLED test pixels patterned on PET/ITO demonstrated that straining the devices 3-4 % tensile (D=0.5 cm) had negligible effect on OLED performance. Flex tests on unpatterned barrier coated PET (PET/FG500 without ITO), on the other hand, showed that the barrier film suffered severe cracking when bent around D=1.2 cm, but no visible cracks were observed for D=2.6 cm. Further experiments performed on rows of ITO lined with metal buslines, such as might be found in a passive matrix display, revealed significant cracking in both the ITO and busline regions. Overall, the results of the flexibility tests indicated that OLEDs are far less vulnerable to the strain induced by flexing than the underlying Barix™ film and ITO anode. Strain on the ITO can, however, be reduced through appropriate patterning.

Construction of an automated flex tester was completed at UDC in 2002Q1. Subsequent flexibility tests were carried out using the automated tester. Flex testing of thin film encapsulated OLED displays on barrier coated plastic substrates performed in 2002Q2 showed that the *overlying* Barix™ film also suffers when the encapsulated FOLED display undergoes tensile stress. The coating, however, can be modified to endure the stress. Figure 16 shows post-test pictures of a PM-FOLED display (317 μm, 64x240 pixels) monolithically encapsulated with only a thin polymer smoothing layer after being flexed 1000 times around a 1-inch diameter mandrel. The mandrel was placed parallel to the 240 columns. The pictures show that severe cracking and delamination of the barrier coating occurred as a result of the tensile stress.

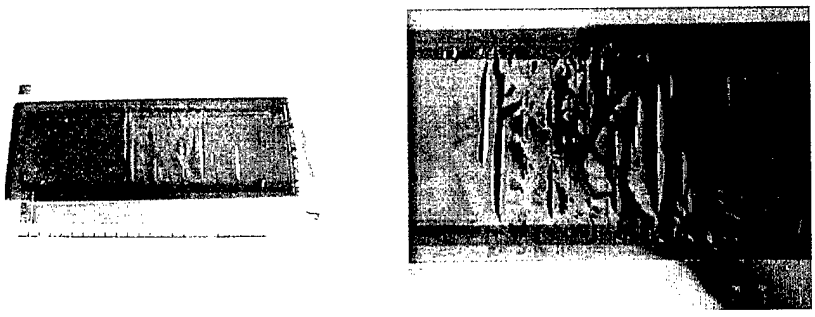

Figure 16: Post-test pictures of a monolithically encapsulated FOLED display with a thin polymer smoothing layer after the display was flexed 1000 times around a 1-inch diameter mandrel.

The barrier coating fared better, however, when the thickness of the polymer smoothing layer was increased. Figure 17 shows before and after pictures of a monolithically encapsulated FOLED display (same type as in Figure 16); the display was flexed 1200 times around a 1-inch diameter mandrel. The results indicate that the flexibility of Barix™ coated displays can potentially be tailored to a desired flexing specification. Further work will be required, however, to optimize both the barrier properties and flexibility of monolithically encapsulated displays.

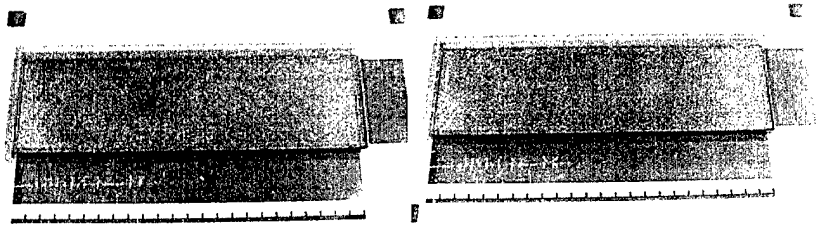

Figure 17: Photographs of a monolithically encapsulated display before (left) and after (right) the display was flexed 1200 times around a 1-inch diameter mandrel. The polymer smoothing layer on the barrier coating of this display was approximately 2 μm thicker than that on the display in Figure 13.

3.1.8 Near-Infrared Emission of Green and Red PHOLEDs

Figure 18 shows the electroluminescence spectra (400-950 nm) typical of UDC's green and red PHOLEDs. The peak wavelength for green emission is 514 nm; the peak wavelength for red emission is 616 nm. As shown in Figure 18, electroluminescence from both PHOLEDs is negligible in the near-IR region.

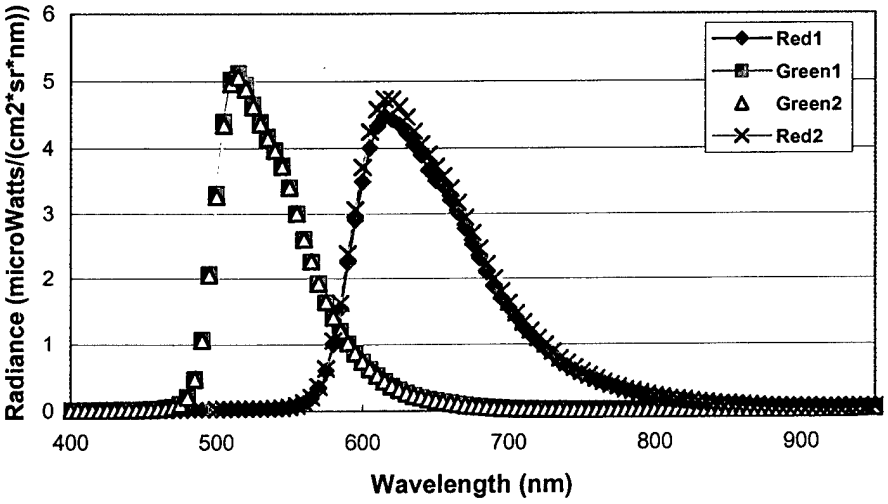

Figure 18: Electroluminescence spectra of red and green PHOLEDs showing negligible emission in the near-IR region.

3.1.9 Thermal Cycling and Humidity Tests

Two red and two green OLED slides with an emissive area of 1 cm^2 were run through a thermal cycle test and a humidity test. The serial numbers for the units under test are as follows: 6-122601-1 XIII and VX (green), 6-112801-1 II and III (red). The environmental chambers were configured so that the units could be powered up and observed while under test. The OLEDs were first scanned by the C-11 spectroradiometer to obtain baseline data. Then the slides were placed in the thermal chamber and alternately heated to 70° C then cooled to –41° C over a twelve-hour period. Throughout the course of this testing the OLEDs were driven at a constant current and the units tested for luminance and chromaticity and voltage. Only small shifts in luminance were observed as the temperature was varied. The OLED device voltages decreased with increasing temperature, as shown in Table II. The data shows that the OLEDs become more efficient at higher temperatures. Table III shows that the OLED luminance and CIE were virtually unchanged by five (5) cycles of thermal stressing from 70° C to –41° C.

Table II. OLED characteristics during thermal stressing.

Unit	Temp (°C)	V	I (mA/cm²)	fL	CIE - x	CIE - y
II (red)	25	7.95	5.02	104	0.641	0.352
III (red)	25	7.97	5.02	103	0.644	0.351
XIII (green)	25	7.1	5.03	194	0.283	0.633
XV (green)	25	6.83	5.04	235	0.28	0.635
II (red)	-40	10.86	5.04	94.4	0.648	0.343
III (red)	-40	10.84	5.02	93.5	0.653	0.341
XIII (green)	-40	9.07	5.04	177	0.284	0.634
XV (green)	-40	9.21	5.06	197	0.284	0.634
II (red)	71	6.57	5.01	102	0.635	0.359
III (red)	71	6.53	5.01	102	0.636	0.359
XIII (green)	71	5.97	5.03	194	0.284	0.629
XV (green)	71	5.7	5.03	242	0.283	0.627

Following the thermal test the same four units were then subjected to a heat and humidity test. The duration of the test was seven full days (168 hrs) and the conditions were 85% relative humidity at a constant 75° C. As before, the units were set in the chamber and powered up and observed while undergoing testing. After 24 hours in the chamber the green units began to show signs of performance degradation, i.e. bright and dark spots, and substantial non-uniformity across the emissive area. The red units fared better but still suffered numerous dark spot defects across the emissive area. The luminance degradation was again very similar to the previous tests where the green units sustained about a 50% decrease in luminance and the red units decreased between 8% and 10%. Further packaging improvements will be necessary for high humidity operation.

Table III: Initial and final OLED data after thermal testing from -40C to +70C for five 12-hour cycles.

Sample	Initial V	Initial fL	Initial CIE	Final V	Final fL	Final CIE
Green	7.95	104	(0.641,0.352)	7.86	105	(0.645, 0.351)
Green	7.97	103	(0.644, .351)	7.92	103	(0.643, 0.351)
Red	7.1	194	(0.283, 0.633)	7.15	197	(0.283, 0.635)
Red	6.83	235	(0.280, 0.635)	6.95	237	(0.282, 0.634)

3.1.10 Display Deliverables

During the course of this program, three passive matrix PHOLED displays were delivered to DARPA. The first during 2001Q3 to Dr. Bob Tulis/DARPA on August 10th and a second to Dr. Darrel Hopper at WPAFB on October 10th. The final display deliverable was made to Dr. Darrel Hopper at WPAFB in August 2002. All display deliverables were made on time.

3.2 Organic vapor Phase Deposition

A second part of the program was to develop a new low cost manufacturing solution for OLED devices. This was based on Organic Vapor Phase Deposition (OVPD) which allows for rapid deposition of small molecular weight organic thin films on continuous flexible backplanes, with a very high material utilization. This Task was to extend the research and development of low cost (e.g. web) processing based on UDC teams' patents on the novel process of low pressure organic vapor phase deposition (LP-OVPD) which allows for very rapid deposition of small molecular weight organic thin films on continuous flexible back-planes.
LP-OVPD offers a unique and realistic method developed only by our team to make very high performance displays using small molecular weight OLEDs on flexible webs in a continuous, roll-to-roll process, overcoming the inherent limitations of conventional vacuum thermal evaporation (VTE).

- VTE is wasteful of organic materials, since deposition occurs on a substrate positioned at least 5 diameters from the evaporation source. Hence, a significant amount of organic source material is deposited onto the chamber walls and not on the substrate, requiring frequent recharging of even very large, production engineered evaporation sources. Materials deposited onto the chamber walls builds up after the completion of several substrate runs. This material flakes off, leading to the generation of particulates, which introduce shorts into the OLED films, thereby reducing display yield.
- Employing flexible substrates based on some polymer materials can result in an elevated background pressure in the VTE high vacuum environment, leading to contamination of the films and chamber. This problem is particularly acute when large surface area substrate coils are mounted into the chamber used for roll-to-roll processing.
- Introducing and removing substrate coils from the VTE vacuum system can be complicated, time consuming and costly.

Fortunately, OVPD suffers from none of these drawbacks. In OVPD organic molecules are heated into a hot carrier gas and deposited onto a cooled substrate. Due to the fact that the OVPD chamber has hot walls and a cold substrate, excess material does not accumulate onto the walls, and hence the chamber does not requiring cleaning to preserve a dust-free environment. Furthermore, the current OVPD reactor designs position the substrate only 1cm distant from the gas injectors, independent of the size of the substrate. Hence, the deposition efficiency (i.e. the amount of organic source material deposited on the substrate to that introduced into the chamber) approaches 100%. Unlike vacuum deposition, recharging of the sources is done by filling containers, which are positioned external to the deposition chamber. Finally, since the chamber design is radically different from that used in high vacuum deposition, and the pressures are ~1 Torr, conversion to roll-to-roll deposition is not complex (as also demonstrated by us in our early experiments on the OVPD growth of OLEDs). OVPD has proved very beneficial for the growth of a range of organic devices, and in particular OLEDs and organic TFTs (OTFTs).

3.2.1 Organic TFTs

OVPD was used very successfully to grow organic TFTs consisting of pentacene channels. By varying both the substrate temperature and chamber pressure, the size of the crystallites could be varied over a substantial range. As the mobility of the OTFT channel is a strong function of crystalline quality, these experiments were necessary to obtain high quality transistor function. At a substrate temperature of 50°C and a chamber pressure of ~10 Torr, an effective channel mobility of 0.6cm^2/V-s was achieved, a value at least as good as the best pentacene results deposited by vacuum on untreated surfaces (as was done in our experiments). Further, varying the chamber pressure to these rather high pressures resulted in crystallite growth with dimensions >10 μm. Given a typical channel length of 1μm, these crystallites extend across the entire OTFT, giving rise to the high performances observed.

By varying both the substrate temperature and chamber pressure, the size of the crystallites could be varied over a substantial range. As the mobility of the OTFT channel is a strong function of crystalline quality, these experiments were necessary to obtain high quality transistor function. We have focussed primarily on surface treatments to initiate crystalline ordering of the pentacene channels. In a factor of 2 improvement over our previous results, an effective channel mobility of 1.3 cm^2/V-s was achieved, a value at least as good as the best pentacene results deposited by vacuum on treated surfaces.

During this program we concentrated on fully understanding the relationship between crystal morphology and film properties as controlled by the process conditions in OVPD growth as well as on surface preparation. The test vehicle for our work was pentacene thin film transistors grown onto OTS treated, as well as untreated silicon dioxide gate dielectric layers. The most important conclusions of these investigations are as follows:

1. As substrate temperature and chamber pressure are increased, while decreasing the film deposition rate, the growth regime shifts from the kinetically controlled, to the diffusion controlled growth process. Diffusion of molecular species to the substrate allows for more equilibrium growth structures to be generated, thereby leading to an increase in crystallite size. The increased crystallite size thus reduces grain boundaries in the

channel, leading to high mobilities and lower drain current on/off ratios. This latter effect is due to increased conductivity through the film bulk due to reduced grain boundaries. Figure 19 shows how the crystallite size in the channel is varied using OVPD. It is further found that the larger the crystal size, the higher the field effect mobility, where we are able to vary this key parameter by an order of magnitude (from 0.06 to 0.6 cm^2/V-s) simply by increasing the crystal grain diameter.

2. If the substrate is pretreated with OTS, the adhesion of the pentacene to the substrate is increased, leading to a higher degree of polycrystallinity (in effect, negating the effects of diffusion limited growth since the molecules are strongly anchored to the substrate once they arrive there during the deposition process). As expected, the drain current on/off ratio is increased due to the high incidence of grain boundaries, but interestingly, the mobility is increased over that obtained with the untreated, large crystallite channels. Indeed, mobilities as high as 1.6 cm^2/V-s are obtained using OTS treated silicon dioxide substrates. X-ray diffraction studies of the treated and untreated substrates imply that there is greater out of plane disorder. Hence, with improved adhesion of the pentacene to the substrate using OTS, it is possible that there is a larger fraction of pentacene molecules lying flat on the substrate, leading to higher mobilities. This result is contrary to conventional wisdom, but is strongly suggested by our results.

In summary, we have found that OVPD can be used to controllably vary organic crystal size, and hence film electronic properties. Further, we find that the performance of OVPD-grown FETs equals or exceeds the very best results reported using other deposition technologies.

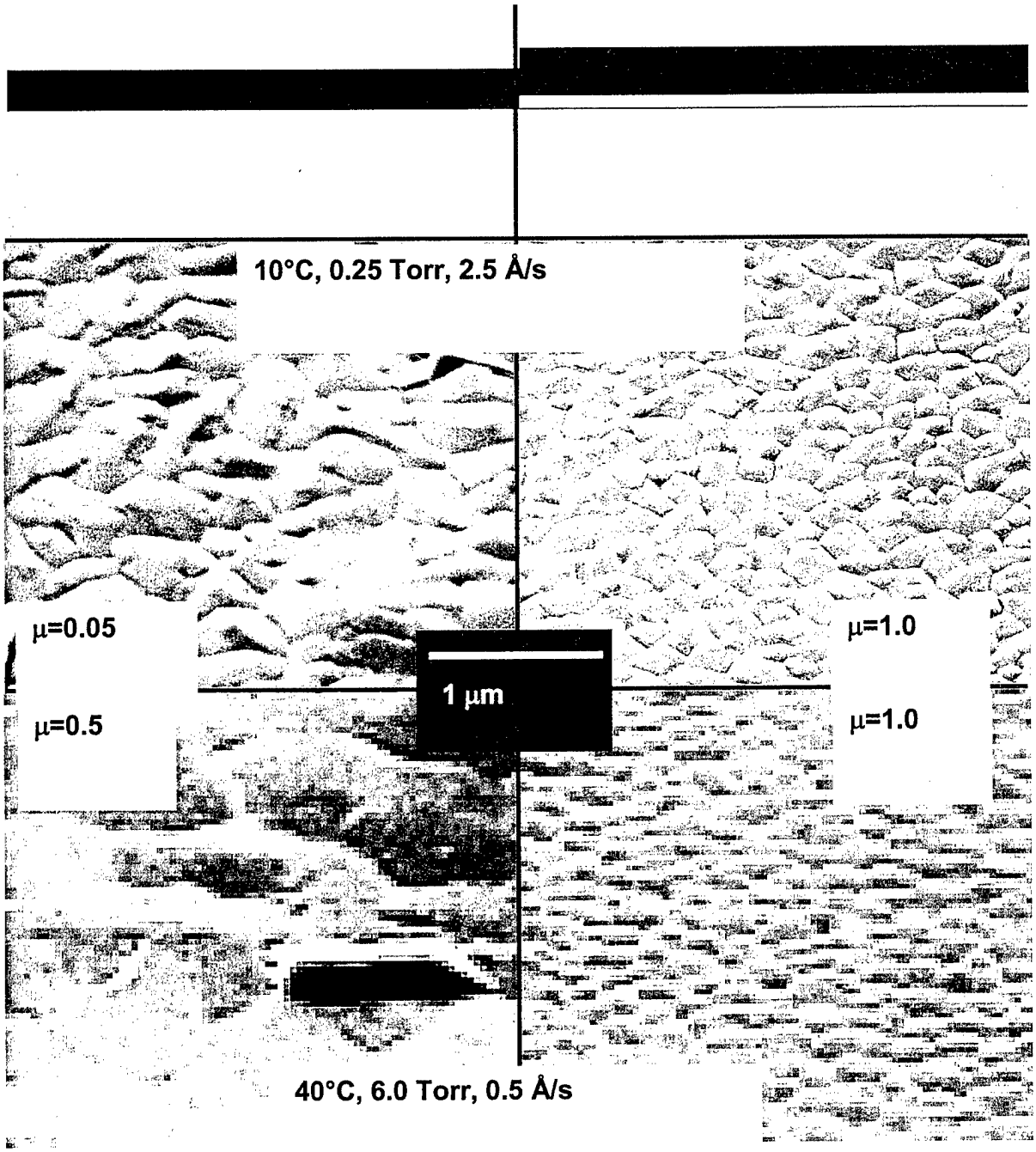

Figure 19: Crystallite size in a TFT channel grown by OVPD for varying deposition conditions.

3.2.2 Simulation of OVPD Film Growth

For the fabrication of full color displays, an important issue for any OLED deposition technology is to quantify patterning during deposition. Initial experimental work focused primarily on deposition through a shadow mask, looking at the limits of patterned deposition. These results indicated a 2-3μm limit for masks positioned within 10 μm of the wafer surface. To gain a deeper theoretical understanding of the process, Monte Carlo routines were established to calculate the deposition pattern beneath a shadow mask, as shown in Figure 20.

The main conclusion from these modelling studies is that the growth through shadow masks is efficiently and simply achieved via growth in the kinetic regime. That is, at the typical pressures employed (0.5 Torr) the mean free path of the molecules is ~5μm, which is ideal for forming high density and high resolution pixels for display applications. Figure 20 shows "computer growth" of approximately 1 μm thick organic film, and find it is well controlled in its lateral dimensions. Following this with vacuum deposition of metals, the metal is fully contained within the pixel area as needed for a non-shorted OLED pixel. The lower panel shows the organic material jets as they emerge through the shadow mask, and their confinement by that mask. The models overall have provided significant insight into the conditions leading to various growth patterns.

This modeling was extended to simulate the OVPD process to further understand the conditions needed for patterned growth of pixels. Hence, we observed both the spreading and deposition efficiency under the following realistic conditions: Mask thickness of 70 μm, aperture width of 80 μm, mean free path = 20 μm (P ~ 0.5 Torr), and carrier velocity of 10 m/sec. The deposition profiles and efficiencies are shown below in Figures 21 and 22.

Overall we make the following observations:

1) The pixel profile appears somewhat domed primarily because of the scale;
2) The "deposition efficiency" was scaled by the fraction of the mask that's "open" - that is, 80 micron aperture / 180 micron center to center spacing gives a simulation = 44.4% .

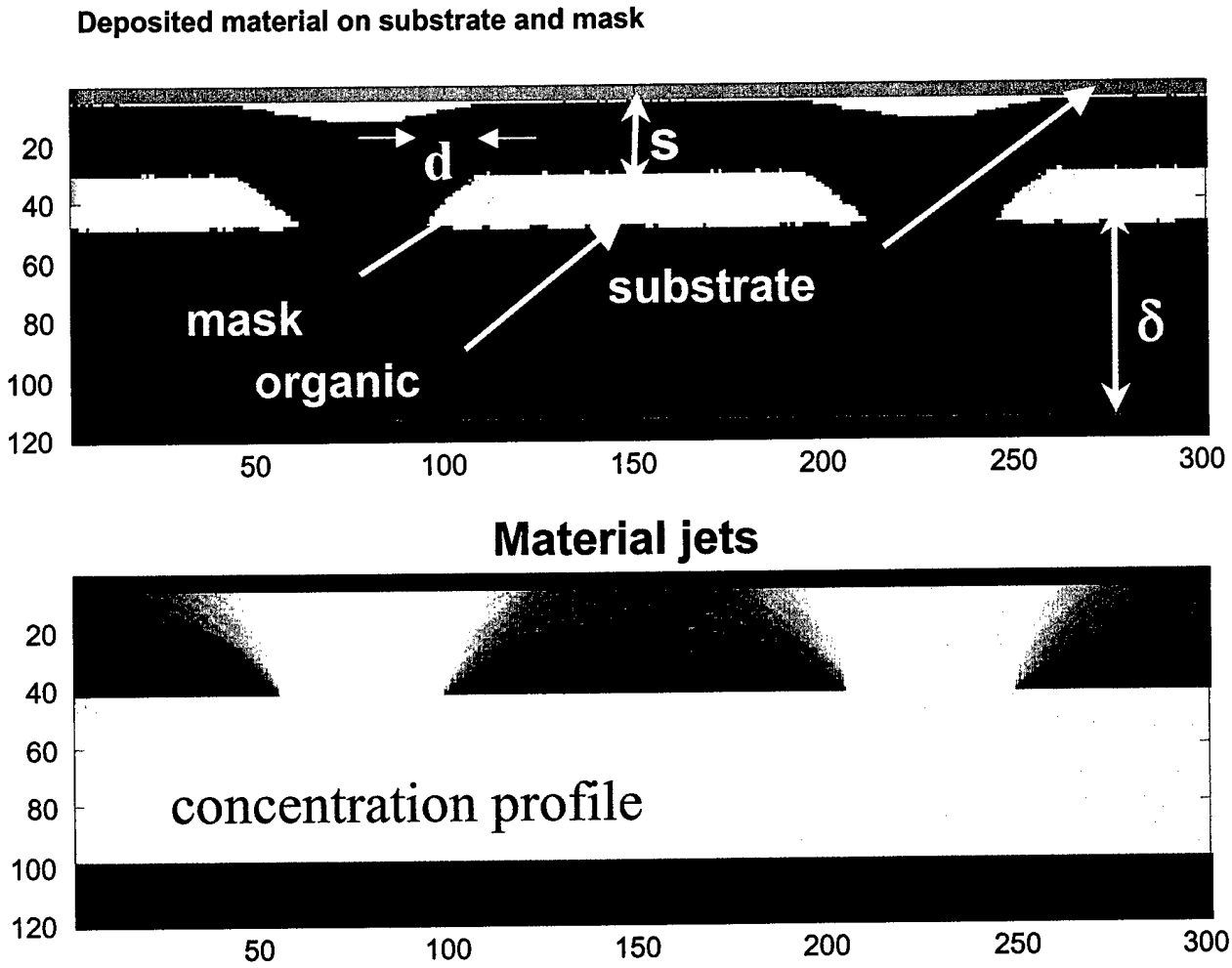

Figure 20: Computer simulations of OVPD growth through a shadow mask (dimensions in μm).

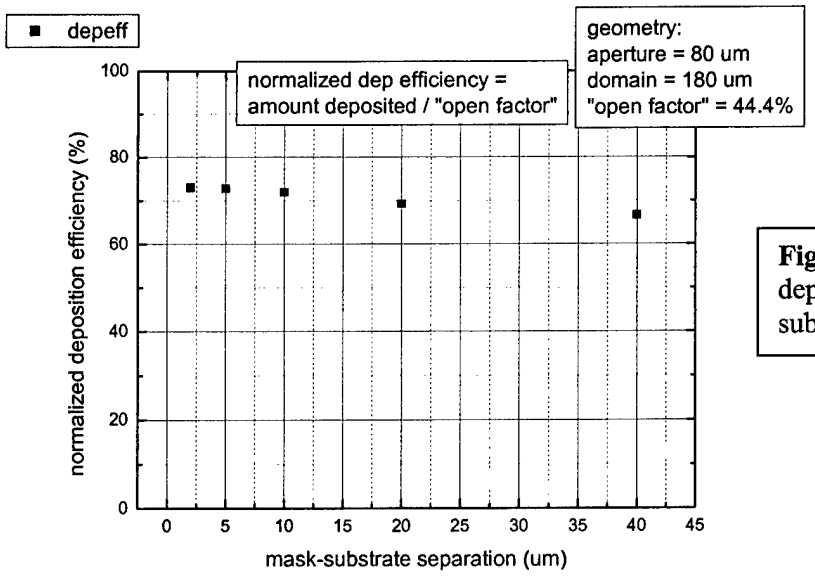

Figure 21: Simulated OVPD deposition efficiency versus mask to substrate separation

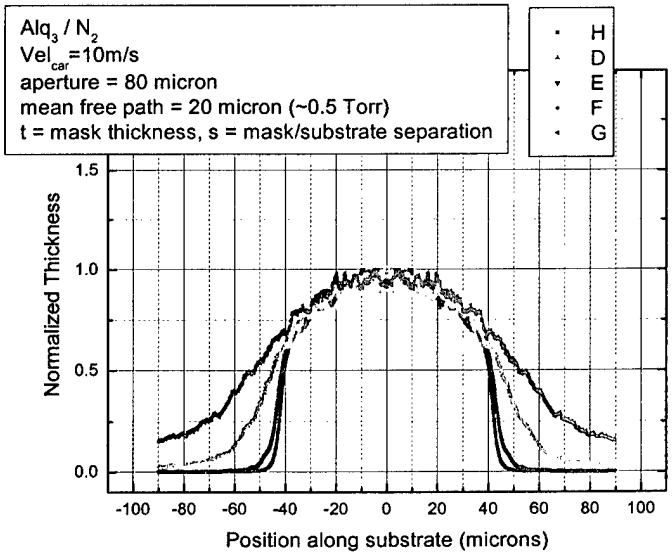

Figure 22: Thickness profile for different mask to substrate separations
D = 2um
E = 5um
F = 10um
G = 20um
H = 40um

3.2.3 Micropatterning of organic thin films using organic vapor phase deposition

For many applications, such as in full color displays, it is often necessary to achieve selective area patterning of the organic film on the substrate via deposition through a shadow mask. Using vacuum thermal evaporation, sharply defined pixels are readily achieved, since the molecular mean free path, λ, at 10^{-7} Torr is ~ 1 m.

On the other hand, OVPD typically proceeds at pressures $>10^{-2}$ Torr, with $\lambda < 1$ cm, resulting in pixels with more diffuse edges. The OVPD concept is illustrated schematically in Figure 23, where diffusion across the boundary layer next to the substrate is shown to limit the deposition rate. Due to the diffusive nature of transport, molecular collisions in the vicinity of the mask and the substrate play a crucial role in determining pattern formation.

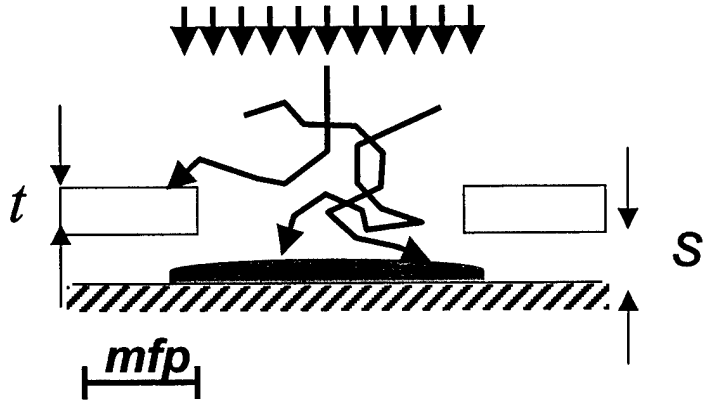

Figure 23: Schematic illustration of OVPD concept

Many modern organic electronic and nanostructure devices require lateral pattern resolution on the order of microns, but are incompatible with conventional photolithography. *In-situ* patterning of the organic films is often used instead. However, Monte-Carlo simulations of patterned OVPD indicate that when the *mfp* is on the order of the pattern size, deposit edges often become less defined. The control of pattern resolution is achieved by varying the *mfp*, the bulk gas flow velocity, and aperture geometry. Simulations and OVPD experiments, both suggest that patterns as small as 1 μm can be achieved, with the deposit profile depending strongly on the aperture shape and distance from the substrate. A weaker dependence on the *mfp* and bulk flow velocity is also found.

In OVPD, the organic source materials are evaporated into streams of a hot inert carrier gas, which transports them toward a cooled substrate where selective physisorption of organics occurs. The macroscopic transport mechanisms of OVPD have recently been discussed, yielding phenomenological models for how process conditions affect deposition rate, doping concentration, and film morphology. The key process parameters include evaporation and reactor wall temperatures (T_{evap}, T_{wall}), carrier gas flow rate ($\dot{V}$), and deposition pressure (P_{dep}), with optimal film deposition conditions characterized by 1 Pa < P_{dep} < 10^3 Pa, 500 K < T_{evap},T_{wall}

< 700 K, and 10 sccm < $\dot{V}$ < 1000 sccm. In this process window, the vapor pressure of the organic molecular species is 10^{-2}-10^{1} Pa, keeping the organic materials volatile yet chemically stable and the gas phase molecular diffusion rate is on the order of the bulk carrier gas flow, promoting film deposition rate and uniformity.

Under optimal OVPD conditions, the molecular mean free path, *mfp*, is typically from 1 to 10^4 μm, the molecular nature of transport and film patterning cannot be ignored. Here, using stochastic simulations and deposition experiments, we examine how deposition conditions and aperture geometry affect the deposited pattern shape. The processing window for OVPD is as follows. The lower bound on the pressure at the source is ~1 Pa. Below this value the pressure drop from the source inlet to the substrate is insufficient to drive the gas flow, and that transport of organics can become diffusion-dominated and poorly controlled. The upper bound to the pressure in the deposition region, P_{dep}, is ~1 kPa, limited by the decreasing diffusivity of organic vapor with pressure. In the pressure range from 1 to 10^3 Pa, the molecular transport changes from the Knudsen regime encountered in vacuum thermal evaporation to the diffusive regime.

Monte Carlo simulations have been employed to study pixel shape dependence on the deposition pressure, *P*, mask-substrate separation, *s*, and mask thickness, *t*. In general, it was found that $s <$ *mfp* (where mfp = molecular mean free path), for acceptably sharp pixels.

More recently, the simulation work has been extended to investigate the effects of mask shape on pixel shape. The best results are achieved using a mask with edges beveled "upward" as illustrated in Figure 24. Here, the deposition efficiency is highest, while pixel edges are the sharpest, due to the small effective separation.

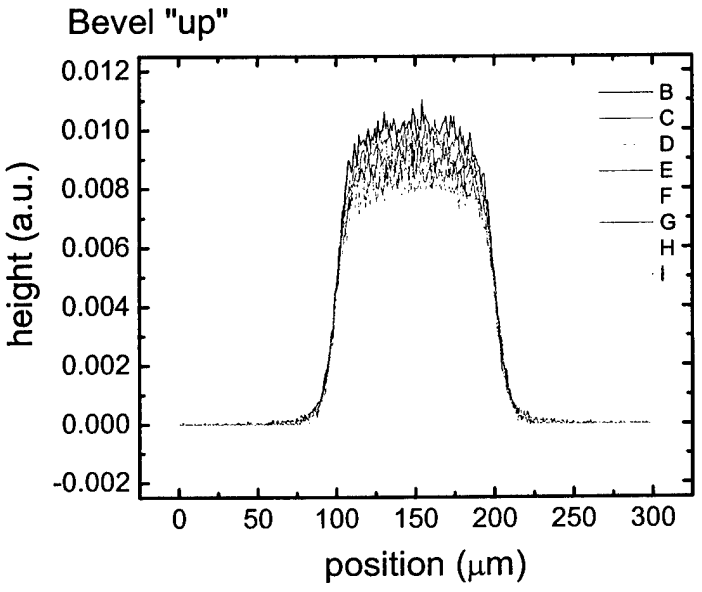

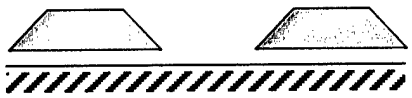

Figure 24: Simulation of pixel shape for a mask with edges beveled upwards for s=20, mfp=20 and t varying from 5 (top curve, B) to 80 (bottom curve, I).

Figures 25a and b show the pixel shapes resulting from OVPD at $P = 0.16$ Torr using cylindrical aperture masks of varying widths, with $t = 60\mu m$ and $s = 0$ and 40 μm. The two depositions are compared for the two 300μm wide apertures in Fig. 25c. The experiment confirms quantitatively that increasing s results in lower deposition efficiency and pixel sharpness.

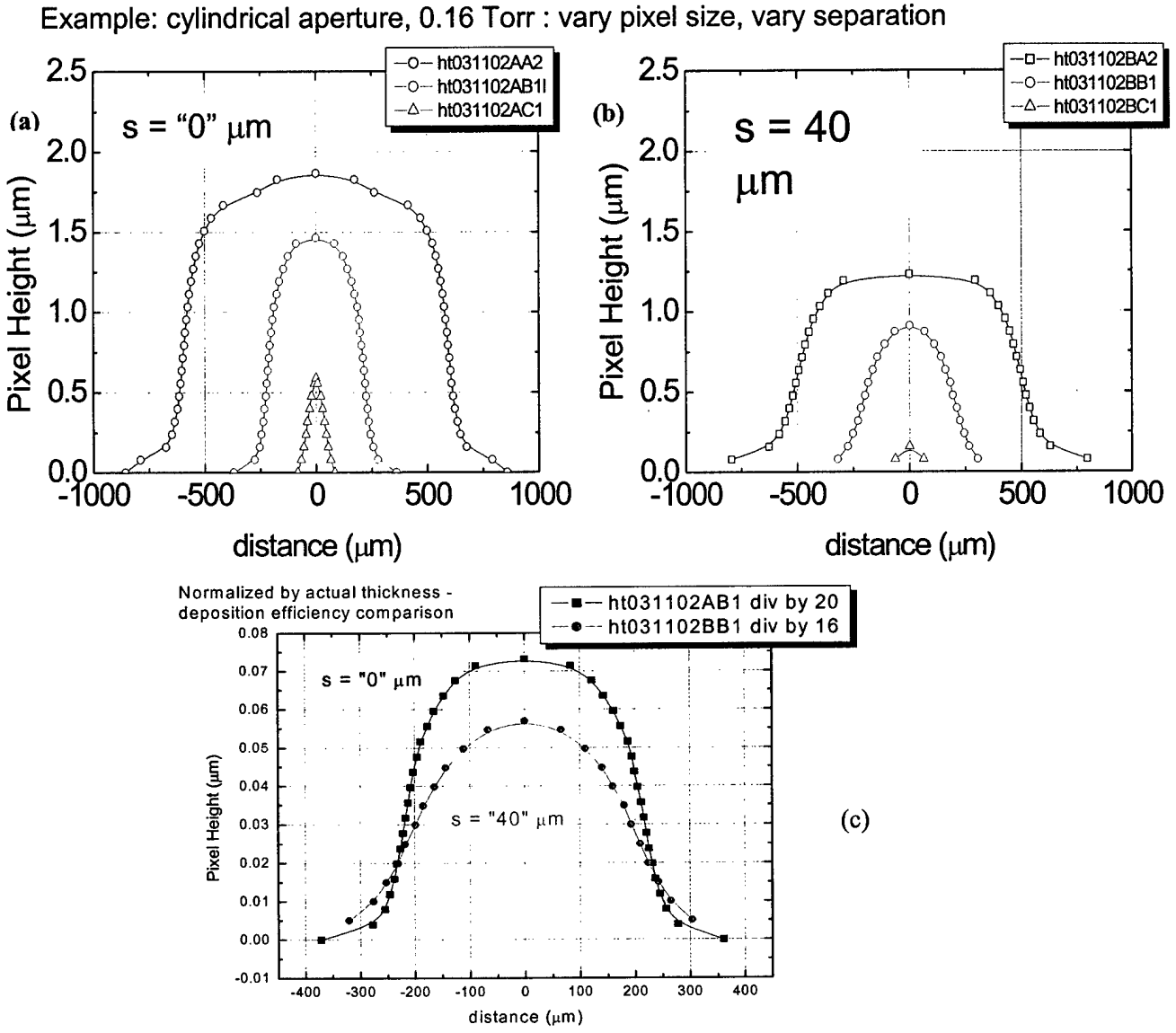

Figure 25: Pixel shapes for cylindrical aperture masks of varying widths with $t = 60\mu m$ and (a) $s = 0$ and (b) 40 μm. Figure 25 (c) compares the two depositions two 300 μm wide apertures.

Figure 26 compares experimental pixel profile for a biconical aperture mask with nominal w = 100μm, t = 75μm, and s = 0+μm to the simulation result of corresponding geometry. The s = 0+ indicates that the mask used in the experiment was actually not in full contact with the substrate during the deposition due to mask roughness and uneven clamping to the substrate (as deduced from pattern variability across the entire substrate). These issues are expected to be resolved in future experiments and commercial application of OVPD.

Figure 27 shows an optical image of 12.5μm wide squares of Alq_3 on Si deposited at P = 1.4 Torr. For this experiment, a 3μm nickel mesh with w = 12.5μm was used. It was clamped firmly to the substrate to minimize s, indicating that even at relatively high deposition pressures, sharp patterns are achievable, provided $s < mfp$.

The simulations and corresponding deposition experiments indicate that pattern definition as small as 1μm is achievable by OVPD. The results help identify appropriate mask geometries, useful processing conditions, and guide the design of future OVPD systems.

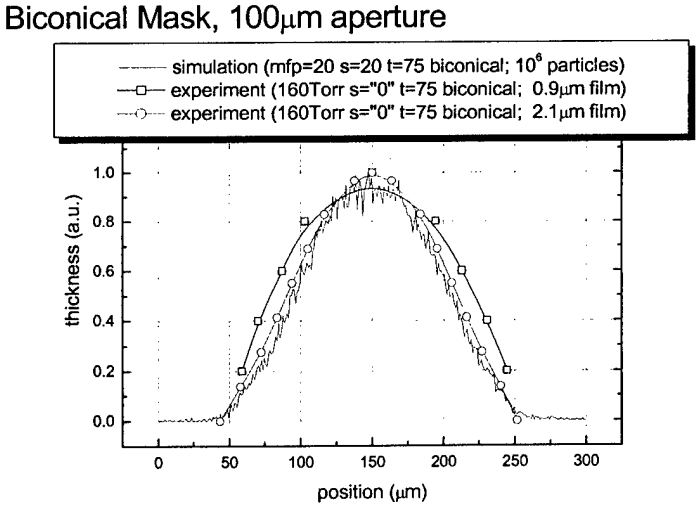

Figure 26: Comparison of experimental pixel profile for a biconical aperture mask with nominal w = 100μm, t = 75μm, and s = 0+μm to the simulation result of corresponding geometry.

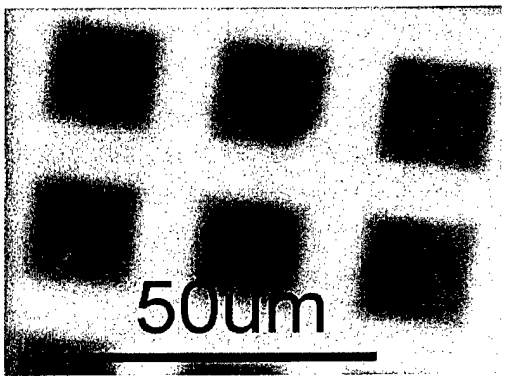

Figure 27: Optical image of 12.5μm wide squares of organic material deposited by OVPD

3.3 Bistable OLED Pixels

Future flat panel displays require a new system architecture which minimizes power consumption and reduces the amount of information to be sent to the display. This can be achieved by fabricating bistable pixels, which only need to be addressed when their state is to be changed i.e. from on to off. In this way, moving parts of the image can be refreshed in real time, whereas static portions are left in their original state without needed to refresh the image on every change of frame. Combined with data compression methods, this can enormously reduce the data I/O to the display backplane, freeing up computer capacity for more complex image and signal processing activities. Phosphorescent OLEDs represent the best and most power efficient means of fabricating bright, low power consumption and flexible flat panel displays. In addition, Princeton University had developed both high efficiency organic photodetectors, and organic TFTs grown by OVPD which exhibit high mobilities comparable to the best vacuum deposited devices. These elements are all the necessary key components for an all organic bistable display pixel.

The OLED device itself produces a light output, which is approximately proportional to the current flowing through it. For very low power consumption, OLEDs require an active-matrix drive architecture, and the OLED current is controlled by placing it in series with a control thin film transistor (TFT). The voltage of the TFT gate therefore determines whether the pixel is on or off. Due to leakage of charge from the TFT gate electrode, in a conventional AMOLED the appropriate video information is "refreshed" or applied to the pixel 60 times per second.

To produce a bistable pixel, we proposed to apply feedback from the OLED to the gate of the control TFT so that its state can be maintained without the need for any refreshing of the video information being sent to the pixel. As the control TFT has gain, only a limited feedback is required to ensure the correct bistable operation. In fact there is a very simple and natural means for providing the feedback in a unique device ideally suited to this program. The feedback element will be a very high efficiency (>85%) fast (450MHz) organic photodiode integrated directly below the OLED. The OLED itself will be our proprietary transparent cathode OLED (or TOLED). By vertical layering of the detector and the TOLED, emission propagating toward the substrate from the TOLED will couple without reflection into the detector layers immediately below it. If the detector is reverse biased, the photocurrent thus generated will flow in the circuit. Using a small gain from the TFT, this photocurrent can then be used to switch the TOLED into the on-state. Since the top contact is transparent, the device is top emitting and hence the viewer has access to the efficient display emission.

The TFTs can be made from organic materials, poly-silicon or amorphous silicon. Whereas our goal was to produce a fully integrated organic bistable OLED display, we recognized that amorphous silicon represented a shorter term backplane solution, due to the existing commercial infrastructure, and also because this technology can be easily adapted to flexible substrates (as compared to poly-silicon). Consequently in this program we developed bistable OLED pixels by pursuing two parallel paths. First, using an amorphous silicon backplane, where we demonstrated the shorter term path of fabricating a small bistable OLED array, and then secondly we further developed our organic technology to demonstrate a fully integrated organic bistable pixel.

3.3.1 All Organic Bistable OLED Pixel

Here, we present an organic photonic integrated circuit (PIC) consisting of an organic photodetector on top of a transparent electrophosphorescent OLED (TOLED). With an external transistor providing positive feedback, bistable switching operation is achieved. Such an integrated device has potential applications for automatic brightness control, image retaining displays (e.g. electronic paper), and other photonic logic applications.

The schematic structure of an integrated transparent OLED (TOLED) device and photodetector (PD) is shown in Figure. 28a. The semi-transparent cathode of the TOLED, consisting of a very thin electron injecting Mg:Ag contact layer capped by a sputter-deposited indium tin oxide (ITO) film, also acts as the anode for the photodetector. Figure 28b shows the representative circuit. Upon reset, the TOLED is subjected to a forward bias, causing its current to increase and emit light. The current in the reverse biased PD increases as the underlying TOLED emits light. This makes the gate voltage of the p-channel FET more negative, leading to an increase in the current passing through the FET and TOLED. Eventually the system reaches the "ON" state when both the TOLED and FET are turned on. The "OFF" state can be initiated by coupling a positive pulse to the transistor gate, turning off the FET, and reducing the TOLED current. This effect will be amplified through feedback from the PD, sustaining the "OFF" state.

A schematic cross section of the PIC is shown in Fig. 28(a). In contrast to reflecting metal cathodes used in conventional OLEDs, the TOLED uses a thin metal layer (~100 Å thick) capped with a sputtered indium-tin-oxide (ITO) layer, which can be >90% transparent. In the integrated device, this intermediate ITO layer also acts as the anode of the photodetector. Here the green electrophosphorescent material, *fac* tris(2-phenylpyridine) iridium [$Ir(ppy)_3$] doped into a 4,4′-N,N′-dicarbazole-biphenyl (CBP) host was used as the luminescent material in the TOLED, while several alternating thin layers of copper phthalocyanine (CuPc) and 3,4,9,10-perylenetetracarboxylic bis-benzimidazole (PTCBI) served as the active region of the organic photodetector.

The bistability of the integrated device is achieved with the addition of an external p-type enhancement-mode Si field-effect transistor FET, and a resistor R, as shown in the circuit of

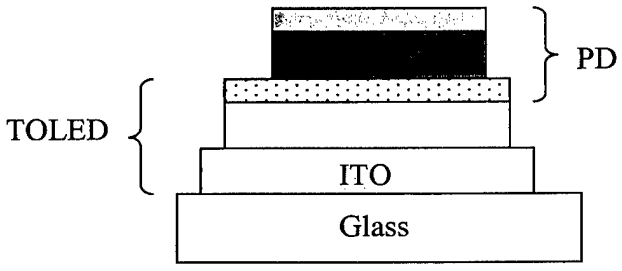

Figure 28a Schematic device structure of an integrated organic bistable switch

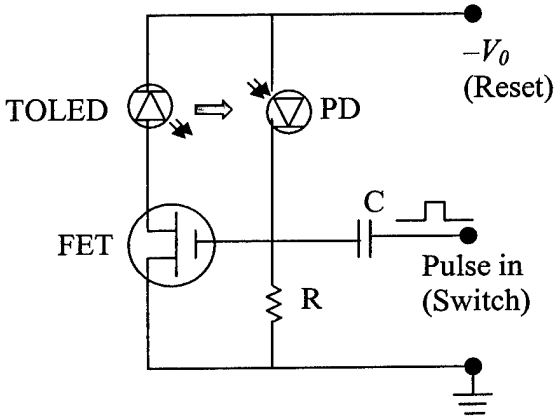

Figure 28b Representative circuit of organic bistable switch

Figure 28(b). There are two possible DC operating points of this system: the "LOW" and "HIGH" states. In the LOW state, the TOLED does not emit light, so that the current passing through the photodetector, I_{PD}, is solely its dark current. By choosing an appropriate value of R, we can have $V_{T1} < V_{g1}^{l} < 0$, where V_{T1} is the threshold voltage of T1, $V_{g1} = -\left|I_{PD}\right| \cdot R$ is the gate voltage of T1, and the superscript "*l*" represents the LOW state. Hence, T1 remains off to maintain the LOW state of the TOLED. In the HIGH state, the TOLED emits green light at a peak wavelength of $\lambda = 515$ nm. The electroluminescent (EL) emission of the TOLED is directly coupled into the photodetector through the transparent cathode of the TOLED, generating a photocurrent. When the total photodetector current is high enough so that $V_{g1}^{h} < V_{T1} < 0$, where the superscript "*h*" represents the HIGH state, T1 is turned on and the HIGH state of the TOLED is maintained. A second "pass" transistor, T2, provides pulses to toggle the switch between HIGH and LOW.

After the ITO sputtering, the sample was transferred into an ultra-high vacuum organic molecular beam deposition chamber with a base pressure of 1×10^{-10} Torr. A 500 Å thick layer of 4,4',4''-tris(3-methyl-phenyl-phenyl-amino)triphenylamine (MTDATA) doped with 2 wt% tetrafluoro-tetracyano-quinodimethane (F_4-TCNQ) was first deposited onto the TOLED cathode. This p-doped layer reduced the dark current of the photodetector while not compromising its quantum efficiency. The photodetector active region, with a total thickness of 480 Å, consisted of 16 alternating layers of 30 Å thick CuPc and 30 Å thick PTCBI, with the first CuPc layer in contact with the MTDATA. A 150 Å thick BCP exciton-blocking layer was deposited on top of the active region. The sample was then transferred to a separate vacuum chamber and a 1000 Å thick Al cathode was evaporated at 1×10^{-6} Torr through a shadow mask with an opening of 0.8×0.8 mm^2 aligned to the center of the TOLED.

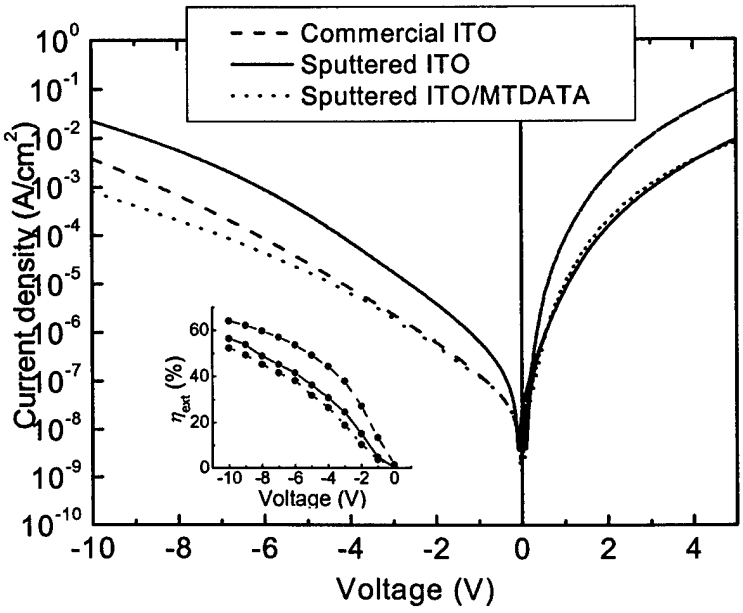

Figure 29: Current-voltage characteristics of photodetectors fabricated on commercial ITO, or sputtered ITO used in the PIC, and with or without a p-doped MTDATA layer between ITO and the first CuPc layer. The inset shows the external quantum efficiencies of these photodetectors at $\lambda = 530$ nm

The dark current of the photodetector under reverse bias increases exponentially with voltage, and as the photodetector is subjected to a larger reverse bias in the LOW state, it is important to suppress the dark current. As shown in Figure 29, when the active region of the photodetector is deposited onto the sputtered ITO anode used in the PIC, the reverse-bias dark current is higher than that obtained using commercial ITO precoated on glass substrates. However, we see a dramatic decrease in the dark current when a p-doped MTDATA layer is inserted between ITO and the first CuPc layer. Shown in the inset of Figure 29 are the external quantum efficiencies, η_{ext}, of the photodetectors, which were measured using a λ=530nm monochromatic beam of light whose intensity was determined with a calibrated Si photodetector. Here, η_{ext} of the photodetector with a sputtered ITO anode is lower by <15% at –10 V than that using a commercial ITO anode, both corresponding to internal quantum efficiencies of close to 100% as the sputtered ITO is approximately 10% less transparent than the commercial ITO.

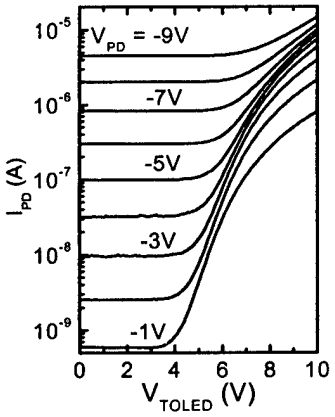

Figure 30: Characteristics of an integrated device: Photodetector current, I_{PD}, as a function of TOLED drive voltage, V_{TOLED}, and photodetector reverse bias, V_{PD};

As shown in Figure 30, at low V_{TOLED}, I_{PD} is predominantly due to the detector dark current, which is 600 pA at –1V, increasing to 4.5 μA at –9 V. Hence at high V_{PD}, V_{TOLED} must be increased to increase the photocurrent well above the dark current. For a discrete TOLED, the luminance of the EL emission through the substrate is P_{bot} = 2300 ± 100 cd/m^2 (or 1.43 mW/cm^2) at 10 V, corresponding to a quantum efficiency of 2.2 ± 0.1 %. The ratio of light emitted through the cathode to that emitted through the substrate is α = 0.50 ± 0.05 for the TOLED with a Mg-Ag layer thickness of 120 Å, resulting in a total quantum efficiency of 3.3 ± 0.2 %. However, with a photodetector integrated on top of the TOLED, nearly 100% of the TOLED top emission is coupled into the photodetector. As shown in Figure 30, the photocurrent is approximately 10 μA with V_D = –9V and V_{TOLED} = 10 V. This corresponds to an absorbed optical power density of 3.6 mW/cm^2 at λ=530nm, while αP_{bot} = 0.72 mW/cm^2 in this case. This enhancement in the extraction efficiency of the TOLED top emission is partially due to the higher refractive index of the photodetector organic layers ($n \approx 1.8$), which is better matched to that of the sputtered ITO than to that of air. Microcavity effects may also contribute to the observed sensitivity enhancement due to the addition of the photodetector and its reflecting Al cathode.

We can estimate the DC operating points of the two stable states of the PIC using Figure 30. Both transistors had threshold voltages of $V_{T1} = V_{T2} = -1.3$ V. With $V_S = -10$ V, in the HIGH state $V_{TOLED} \approx 10$ V, $V_{PD} \approx -7.5$ V, $V_{g1} \approx -2.5$ V $< V_{T1} < 0$, $I_{PD} \approx 11$ μA; whereas in the LOW state $V_{TOLED} \approx 0$ V, $V_{PD} = -9.0$ V, $V_{g1} = -1.0$ V $> V_{T1}$, $I_{PD} = 4.5$μA. To test for proper circuit operation, R = 225 kΩ was connected in series to the photodetector. The voltage drop across the resistor, V_R, was then measured as a function of V_S and V_{TOLED}. $V_R \leq 1$V when $V_S = -10$V and $V_{TOLED} \leq 2$V; whereas 2V $< V_R <$ 3V with $V_S = -10$V and 9V $< V_{TOLED} <$ 10V. As $V_R = -V_{g1}$, these two cases correspond to the LOW and HIGH states of the PIC, respectively.

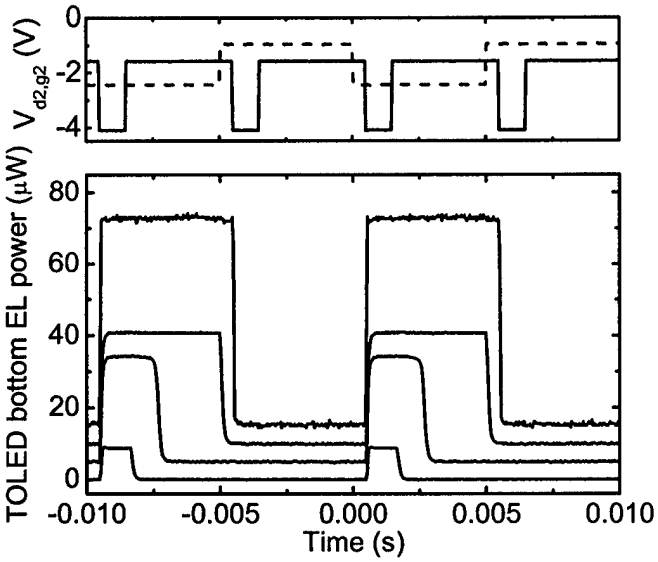

Figure 31: Demonstration of optical bistability of the PIC circuit in Fig.1. Upper panel: waveforms of the switching signals V_{d2} (dashed line) and V_{g2} (solid line). Lower panel: waveforms of the TOLED emission power through the substrate at different V_S (shifted vertically for clarity).

The demonstration of the optical bistability of the PIC is shown in Figure 31, where V_S was varied from –8 V to –10 V. The input of V_{d2} and V_{g2} are shown in the upper panel of Figure 31. Here V_{g2} (solid line) is delayed from V_{d2} (dashed line) by $t_d = 0.5$ ms, and has a pulse width of t_w = 1ms. During the pulse window of V_{g2}, T2 is turned on, setting V_{g1} to –0.95 V or –2.45 V, hence setting the PIC to LOW or reset it to HIGH.

The waveforms of the TOLED bottom EL emission intensity at different V_S are shown in the lower panel of Figure 31 (shifted vertically for clarity). At $V_S = -8$ V, the TOLED is on during the reset window, however, the HIGH state is not stable as the TOLED turns off when T2 is switched off. As V_S is increased, the TOLED remains on for a brief period after T2 is switched off. At $V_S = -9.4$ V, the HIGH state is almost fully latched between two pulses. The stable HIGH state is clearly achieved with $V_S = -10$ V, i.e., the TOLED is turned on at the onset of the RESET window, and remains on until the onset of the SET window, at which time it is turned off and remains off until the next RESET pulse. The RESET or SET windows can be as narrow as 60 ns to make the PIC switch between the two stable states.

The 3dB bandwidth of the bistable pixel circuit is 25 kHz, and the roll-off is approximately –18 dB/decade due to the two poles of the circuit. This represents a lower limit to the actual bandwidth of our device, since the Si photodetector used to measure the TOLED emission

intensity has a response time of ~2 μs. Further, measurements of the capacitances of the circuit elements show that the frequency response is primarily limited by the RC time constant of ≥ 5μs between the TOLED resistance and the transistor capacitance.

3.3.2 Fabrication of Low Dark Current PhotoDetectors

A low detector dark current is very important to ensure that there is a large tolerance in the component values of the feedback circuit which will allow for bistable operation, and a key to the successful demonstration of the optical bistability is that we were able to suppress the photodetector dark current while achieving very high efficiency from it. The multiplayer CuPc/PTCBI photodetector can be very efficient (Peumans, et al., Appl. Phys. Lett. 76, 3855 (2000)). When 16 alternating layers of 30 Å thick CuPc and 30 Å thick PTCBI were directly deposited onto a sputtered ITO anode which in the integrated device also serves as part of the transparent cathode of the underlying TOLED, we showed that the internal quantum efficiency approached 100% at an applied bias of –10 V. However the reverse-bias dark current of the photodetector was at least an order of magnitude higher than that for a similar device fabricated on a commercial ITO anode. We inserted a 500 Å thick p-doped MTDATA layer between the sputtered ITO and the first CuPc and observed a dramatic decrease in the dark current while the quantum efficiency is only reduced by <5%.

In continuing the work, we attempted to understand why this p-doped layer helped to reduce the photodetector dark current and also look for ways to optimize the photodetector performance.

1. Atomic force microscopy studies of film morphology

We used atomic force microscopy (AFM) to study the surface morphology of commercial and home-sputtered ITO films. As shown in Figure 32, the commercially obtained ITO film (left image) has clustered grains with size of approximately 300 nm, and the root-mean-square (RMS) roughness is 1.0 ± 0.2 nm. The home-sputtered ITO film (right image) has much smaller grains, ~80 nm in size, with a smaller RMS roughness of 0.4 ± 0.1 nm. Therefore it is not due to the difference in surface morphology that a photodetector with a sputtered ITO anode has higher dark current than one with a commercial ITO.

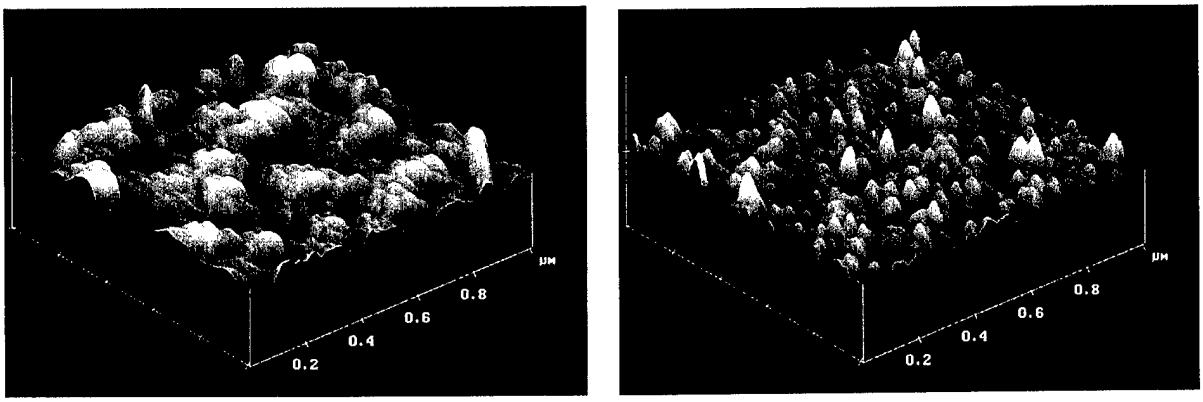

Figure 32: AFM micrographs of a commercial (left) and a home-sputtered (right) ITO film. The scan size is 1 μm × 1 μm, and the vertical scale is 10 nm/div.

3.3.3 Dark current of various photodetector structures

For the detector with a commercial ITO anode, the dark current densities at applied biases of –10 V (filled symbols) and –5 V (open symbols) are shown in Figure 33 as a function of the device operating temperature. Clearly the dark current is thermally activated with an activation energy of 0.24 eV at –10 V or 0.37 eV at –5 V for T > 200 K. On the other hand, as also shown in Figure 33, the external quantum efficiency (η_{ext}) of such device is less dependent on the temperature although it also decreases with temperature. At –5 V, the activation energy for η_{ext} is only 0.07 eV, whereas η_{ext} at –10 V is almost constant over the temperature range of 200 K < T < 320 K. For the detectors fabricated on commercial ITO with different organic layer structure, as shown in Figure 34, the dark current under reverse bias have two regimes: at high bias (V < –4 V) the dark current increases as increasing the number of hetero-interfaces or reducing the layer thickness, while at low bias (–2 V < V < 0) the dark current tends to be the lowest for the detector with the most number of hetero-interfaces or the thinnest layers of CuPc and PTCBI.

It is difficult to interpret all these results and we have yet come up with a model of charge generation and transport in these devices. Nevertheless, a few conclusions can be drawn based on the current data.

First, the weak dependence of η_{ext} on temperature for the detector with 30 Å thick CuPc and PTCBI layers indicates that the photo-generated carriers can tunnel through the barriers formed by the hetero-interfaces, i.e. holes in the CuPc HOMO can tunnel through the PTCBI layer whereas electrons in the PTCBI LUMO can tunnel through the CuPc layer. The small activation energy observed for η_{ext} could be associated with the exciton diffusion process.

Under reverse bias, the generation-recombination current in the depletion region could be a major component for the dark current. Charge carriers can be generated within each depleted organic layer, at the organic-organic interfaces, or at the organic/electrode interfaces. The generation rate inside each CuPc or PTCBI layer is proportional to $\exp(-E_g / 2kT)$, where E_g is the HOMO-LUMO gap of CuPc or PTCBI. At a CuPc/PTCBI interface, the generation rate could be higher because E_g is reduced by the HOMO or LUMO offset between CuPc and PTCBI which is approximately 0.7 eV. This could possibly explain the reason that at sufficiently high reverse bias the photodetector with thinner CuPc or PTCBI layers has higher dark current. Another possible reason for that is that with thin layers (such as 30 Å thick) these generated charge carriers can tunnel through the barriers formed by the hetero-interfaces, much like the way photo-generated carriers do, but with thicker layers the tunneling probability is significantly reduced and thermionic emission over these barriers is the dominant transport mechanism. This can be verified by the lower quantum efficiency of detectors with each layer thicker than 40 Å (see Peumans et al., Appl. Phys. Lett. 76, 3855 (2000)).

To explain the effect of different ITO anode on the dark current for the detector with 30 Å thick CuPc or PTCBI layers, we need to consider the possibilities of carrier injection from electrodes. Under reverse bias it is unlikely that holes can be injected from the cathode because they need to overcome the large barrier of ~ 2 eV between the HOMO of BCP and the Fermi level of Al. At the ITO/CuPc interface, however, if the work function of ITO is low, such as in the case of home

sputtered ITO, it is possible that electrons tunnel through a thin CuPc layer into the LUMO of PTCBI. This tunnel current can be cut off either by increasing the first CuPc layer thickness or by increasing the anode work function (such as treating ITO in a O_2 plasma or coating ITO with a p-doped MTDATA layer).

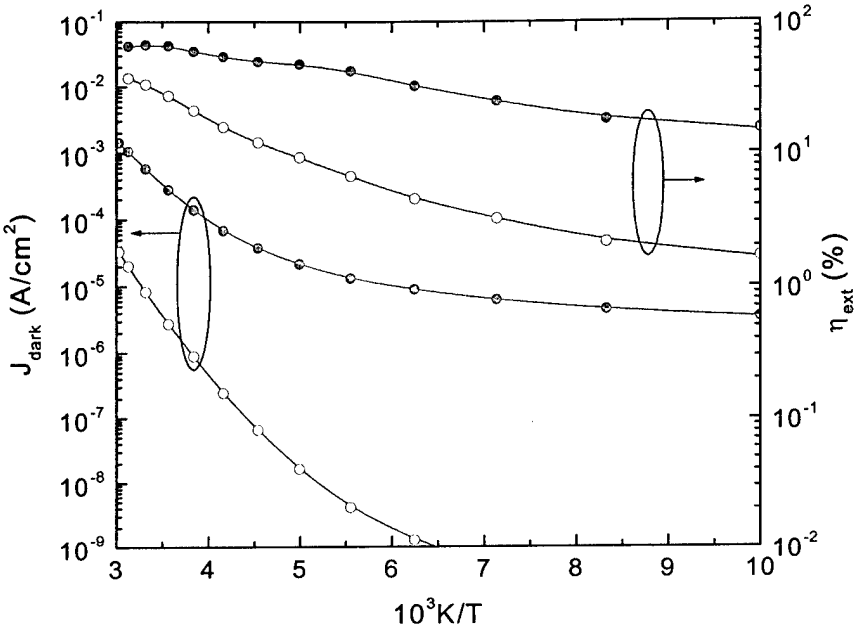

Figure 33: Dark current density and external quantum efficiency (at λ = 633 nm) measured as a function of temperature for a photodetector with a structure of commercial ITO/[CuPc(30Å)/PTCBI(30Å)]$_8$/BCP(150Å)/Al. Filled symbols correspond to an applied bias of –10 V while open symbols correspond to –5 V.

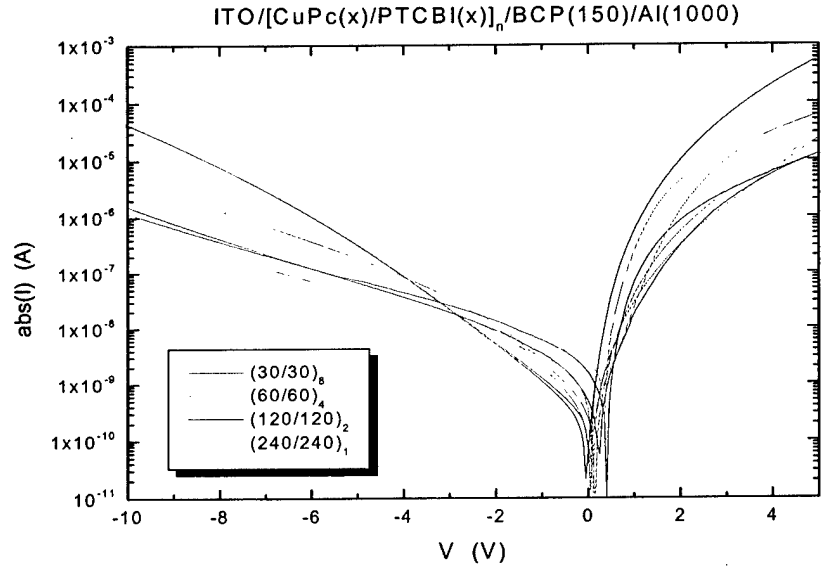

Figure 34. Comparison of the dark current for photodetectors with different organic layer structures. All detectors were fabricated on commercial ITO anodes.

3.3.4 Bistable OLED Pixels based on Amorphous Silicon Backplanes

The objective of this task was to design and fabricate a 20×20 array of bi-stable (1 bit gray scale) a-Si thin film transistor (TFT) OLED active matrix pixels. This work combined UDC's phosphorescent OLED technology with conventional amorphous silicon backplane technology. The a-Si TFT's provided by the electrical gain to maintain the pixel in a given state, and by virtue of their high photoconductivity, these devices also operated as photodetectors.

Two different approaches were taken to achieve bi-stability, optical and electrical feedback. Schematics of both the optical and electrical feedback bi-stable pixel designs are shown in Figure 35. Both designs contain a select and OLED drive TFT as would be found in a conventional two-TFT per pixel OLED display. The optical feedback pixel uses an additional pull-up and pull-down TFT, each having a non-gated gap in the channel region (split-gate) connected so that V_{GS} is positive for each device, to retain the pixel state. When the pixel is in the off state, both the pull-up and pull-down TFT have very high impedance due to the non-gated region of the channels. By making the channel width to length ratio of the pull-down TFT larger than that of the pull-up TFT, the impedance of the pull-down TFT is less than that of pull-up TFT and the V_{GS} for the OLED drive TFT is pulled to a small value and the OLED remains off. This condition, once set by the select transistor, is stable and the pixel requires no additional input to retain the state.

When the pixel is turned on, the emission of the OLED is coupled to the channel of the pull-up TFT. Charge carriers are optically generated in the channel and its impedance is greatly reduced. Because the drain of the pull-up TFT is connected to a positive voltage, V_{GS} for the OLED drive TFT is pulled high and the OLED remains lit when the select TFT is turned off. The position of a small OLED (separate from but in parallel with the main pixel OLED) directly over the channel of the pull-up TFT provides efficient optical coupling and eliminates the need for wave guiding techniques. A cross-section of the split-gate pull-up TFT is shown in Figure 36. The use of a split-gate allows for the entire high impedance (non-gated) portion of the channel to be illuminated, avoiding shielding from the source/drain metal overlap. The pull-down TFT uses a split gate configuration to allow equal illumination of the channels of the pull-down and pull-up TFTs from ambient light. This is especially important during the off state when ambient illumination of the pull-up TFT only, could reduce it's impedance to a value less than that the pull-down TFT, causing V_{GS} of the drive TFT to be pulled high, turning the pixel on.

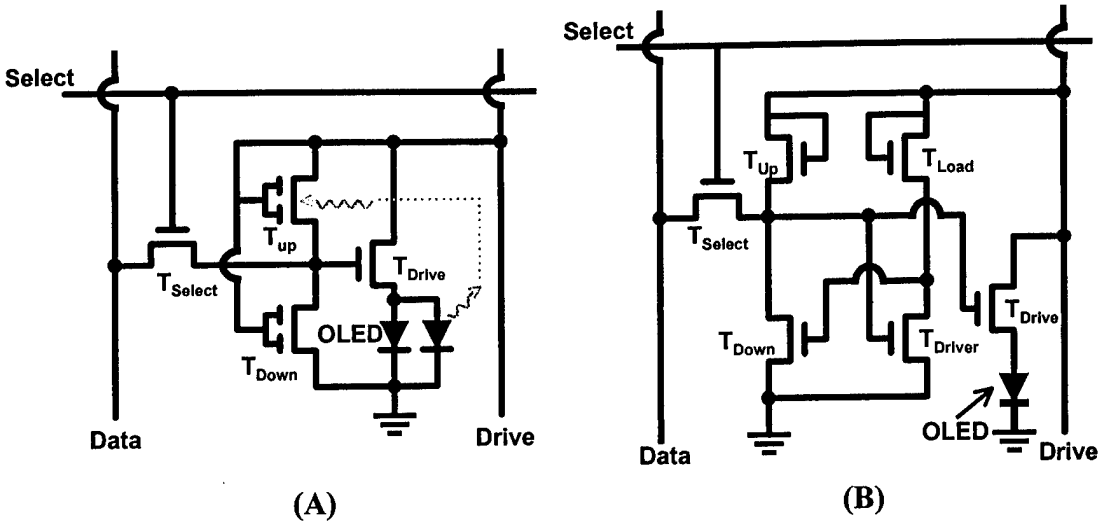

Figure 35: Schematics of A) optical and B) electrical feedback bi-stable pixels.

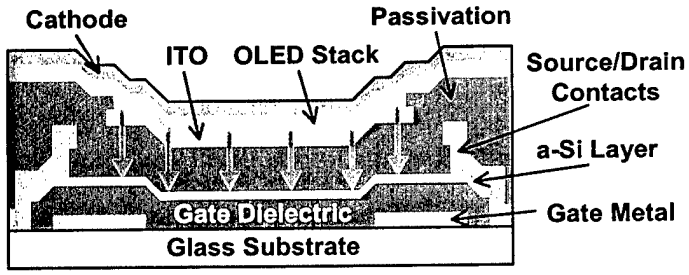

Figure 36: Cross-section of split-gate pull-up TFT used in optical feedback bi-stable pixel.

The electrical feedback pixel consists of six TFTs, four of which are used to form a latch that holds the pixel in either the on or off state. It has the advantage of remaining stable even at reduced OLED drive voltages however current flowing through latch makes a separate ground connection necessary. Optical micrographs of the TFT layout for both the optical and electrical feedback pixels before OLED stack and cathode deposition are shown in Figure 38.

The mask layout, Figure 37, included four 20×20 arrays of one millimeter pixels, individual pixels, TFTs, and several test structures.

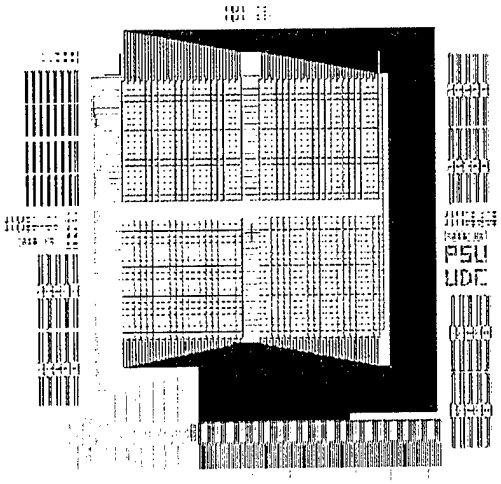

Figure 37: Bi-stable pixel mask layout.

3.3.5 Fabrication Process for a-Si/OLED array

A inverted staggered tri-layer a-Si:H process with a maximum process temperature of 300 °C was used for pixel fabrication on glass substrates. First, a 75 nm ion-beam deposited chromium (Cr) film was patterned to define the gate metal. The trilayer stack was deposited by plasma-enhanced chemical vapor deposition (PECVD) and consisted of a 300 nm silicon nitride (SiN) gate dielectric (substrate temperature = 300 °C), 50 nm intrinsic a-Si:H active layer (T_{sub} = 250 °C), and 300 nm SiN layer (T_{sub}=250 °C). Photolithography and etching were used to form the active region and contact vias were etched to the intrinsic a-Si:H layer. For source/drain contacts, a 50 nm n^+ microcrystalline silicon (μc-Si) layer was deposited by PECVD (T_{sub} = 250 °C) followed by 200 nm of sputtered molybdenum (Mo). The Mo film was patterned and etched and then used as a mask during etching of the n^+ μc-Si. With the TFT fabrication completed, a 300 nm SiN passivation layer (T_{sub} = 250 °C) was then deposited, vias were etched, and 200nm of ITO was deposited by sputtering. The ITO was photolithographically patterned and etched to form the pixel anode. Finally, a second passivation layer was deposited and holes were opened down to the ITO anode and metal contact pads.

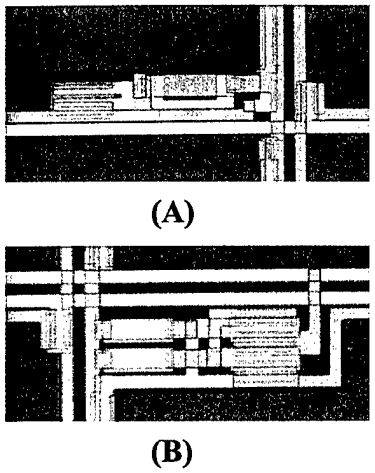

Figure 38: Optical micrographs of TFT layout for A) optical and B) electrical feedback bi-stable pixels.

The OLED stack was deposited onto the TFT backplane by thermal evaporation in an OLED deposition system with base pressure < 5×10^{-8} torr. The organic layers were: 20 nm copper phthalocyanine (CuPc) as the hole injection layer, 30 nm 4,4'-bis[N-(1-napthyl)-N-Phenyl-amino] biphenyl (α-NPD) as the hole transport layer, 30 nm 4,4'-N,N'-dicarbazole-biphenyl (CBP) doped with 6 wt% of *fac* tris(2-phenylpyridine) iridium [$Ir(ppy)_3$] as the emitting layer, 10 nm aluminum(III) bis(2-methyl-8-quinolinato)4-phenylphenolate (BAlq) as the hole blocking layer, and 40 nm tris (8-hydroxyquinoline) aluminum (Alq_3) as the electron transport layer. Next, a 1 nm lithium fluoride electron injection layer and an aluminum cathode were deposited. The arrays were encapsulated with a glass cover plate.

3.3.6 Results of a-Si/OLED arrays

Optical Feedback Bi-stable pixel

In the initial optical feedback bi-stable pixel design, the silicon nitride gate dielectric layer was used to guide the light from the OLED pixel to the pull-up TFT (Figure 39) while the pull-down TFT was shielded from ambient and stray pixel light using standard optical wave-guide techniques such as opaque

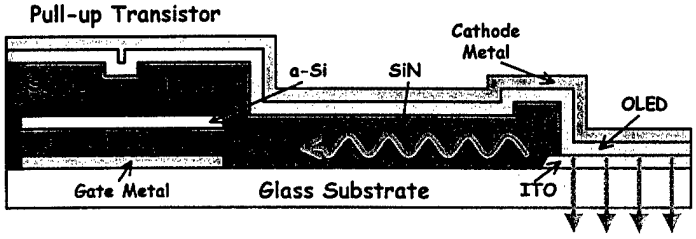

Figure 39: Cross-section of pull-up TFT that used light guiding for coupling with OLED.

stop layers or lossy metal cladding layers. Measurements on test structures showed little current modulation in the pull-up TFTs between when the OLED was on and off, a possible result of poor guiding and/or coupling of the light. The problem was believed to be enabling the OLED light to enter the silicon nitride and/or into the a-Si active layer, not an attenuation of the light in the guide. The techniques used for shielding light from the pull-down TFT, did appear to be effective. The coupling also may have been poor because the entire channel of the pull-up TFT was gated, with the gate connected to the source.

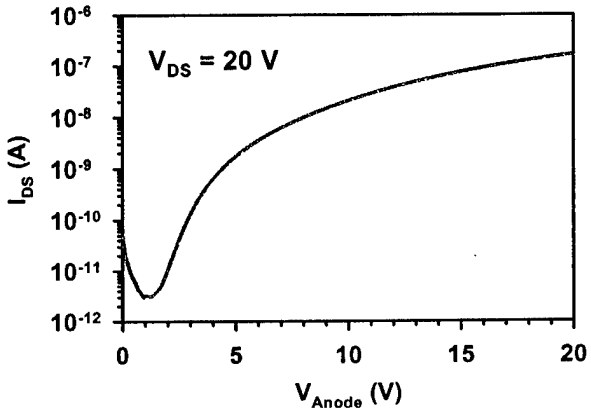

Figure 40: I_{DS} plotted versus V_{Anode} for split-gate pull-up TFT with OLED fabricated over channel.

Improved performance was obtained using a split-gate pull-up TFT with the OLED placed directly over the channel. For test devices (Figure 40), several orders of magnitude modulation in I_{DS} was seen when the OLED bias was increased. The pixels were tested for bi-stability by pulsing a select and data voltage and watching to see if the OLED remained on. The OLED current is plotted versus time for an optical feedback bi-stable pixel in Figure 41. The pixel was initially off (V_{select} = V_{data} = 0 V, V_{drive} = 20 V). At t = 2 seconds, the OLED was turned on by quickly pulsing the data and select voltages (V_{select} = V_{data} = 20 V, V_{drive} = 20 V). After the pulse, the data and select voltages were returned to zero (V_{select} = V_{data} = 0 V, V_{drive} = 20 V) and the OLED remained lit. However, the pixels would slowly (tens of seconds) dim and eventually turn completely off. This instability was strongly influenced by the amount of ambient light with brighter conditions causing the pixel to decay faster to the off-state. A comparison of a pixel tested under dark conditions and while illuminated by a microscope light is found in Figure 41. Figure 42 shows an image of lit optical feedback bi-stable pixel. The small OLED fabricated over the pull-up TFT can be seen in the upper right.

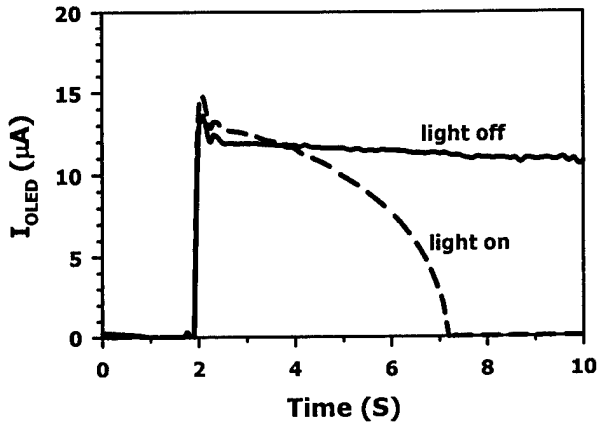

Figure 41: I_{OLED} plotted versus time for microscope light on and off conditions.

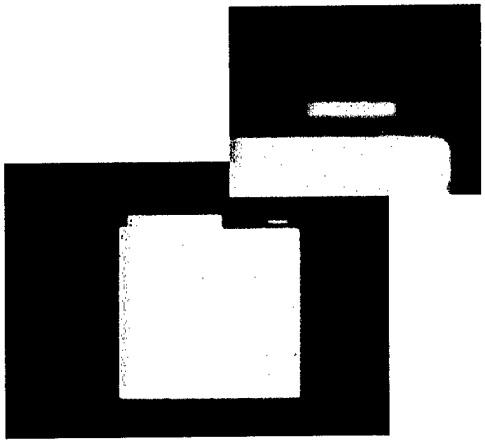

Figure 42: Optical micrograph of lit optical feedback bi-stable pixel.

The performance of the optical feedback bi-stable pixel most likely could be improved with minor modifications to the pixel design. For instance, by connecting the split-gate of the pull-down TFT to the gate of the drive TFT (Figure 43) instead of to OLED drive would reduce V_{GS} for the pull-down TFT when the pixel is in the on-state and may improve stability. Increasing the un-gated channel length of the pull-down TFT may also eliminate the on-state decay by reducing the density of carriers generated in this region by the split-gate's electric field.

Electrical Feedback Bi-stable Pixel

The electrical feedback pixels showed excellent bi-stability. The OLED current is plotted versus time in Figure 44. The pixel was initially off (V_{select} = V_{data} = 0 V, V_{drive} = 30 V). At five seconds, the OLED was turned on (V_{select} = V_{data} = 30 V, V_{drive} = 30 V) and an OLED current of 6 μA was measured. At ten seconds, the select and data voltages were returned to zero (V_{select} = V_{data} = 0 V, V_{drive} = 30 V) and the OLED remained lit with a current of 5 μA. The pixel retained its state indefinitely as long as a sufficient (a few volts) OLED drive was applied. A large current (1 μA) through the latch was measured but could be reduced by optimizing the pixel design. This current is undesirable not only because of power consumption but also because it makes it necessary to include an additional grounding line.

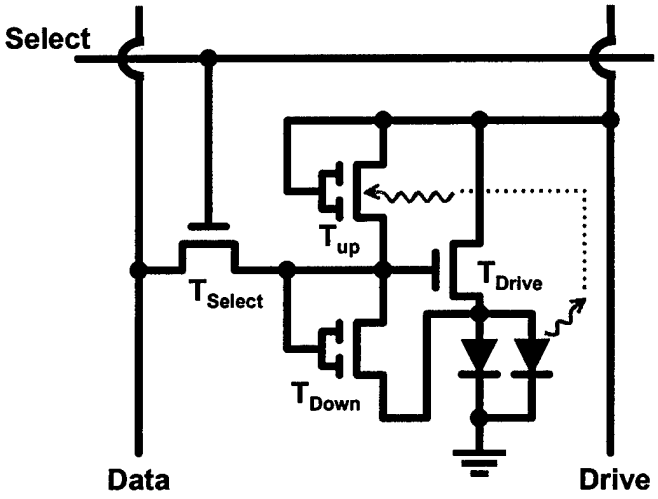

Figure 43: Schematic of newly designed optical feedback bi-stable pixel.

20×20 Arrays

The response of the arrays was examined by driving them with conventional active matrix OLED electronics. While there were numerous defects, the arrays were able to display images. Figure 45 shows both the optical and electrical feedback arrays displaying a checkered board pattern. The bi-stability of the arrays was tested with the drive electronics detached by tying lines together so that there were only four connections (select, data, OLED drive, and cathode) needed

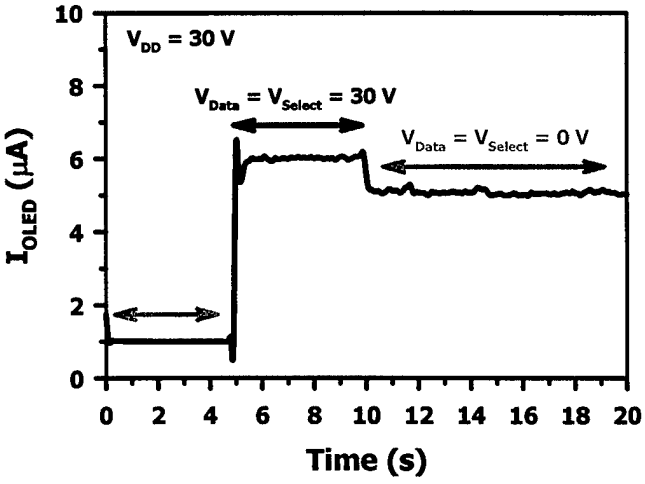

Figure 44: I_{OLED} plotted versus time for electrical bi-stable pixel.

to drive all the pixels in the array. For the electrical feedback bi-stable array, the testing began with the pixels off ($V_{select} = V_{data} = 0$ V, $V_{drive} = 15$ V). The pixels were turned on by pulsing the select and data lines ($V_{select} = V_{data} = 15$ V, $V_{drive} = 15$ V) and remained on after the pulse ($V_{select} = V_{data} = 0$ V, $V_{drive} = 15$ V). The OLED drive was then lowered until the pixels no longer emitted light ($V_{select} = V_{data} = 0$ V, $V_{drive} = 4$ V) and held there for several seconds. When the OLED drive was increased back to the original bias ($V_{select} = V_{data} = 0$ V, $V_{drive} = 15$ V), the pixels returned to the on state. Figure 46 shows images of the array taken at different moments during testing.

Similar testing of the optical feedback bi-stable pixel arrays further demonstrated the on-state decay previously seen in the testing of individual pixels. The stability was improved by operating the array at low OLED drive voltages. To demonstrate the light sensitivity of the optical feedback pixels, the entire array was pulsed to the on state and a laser pointer was used to turn off illuminated pixels (Figure 47).

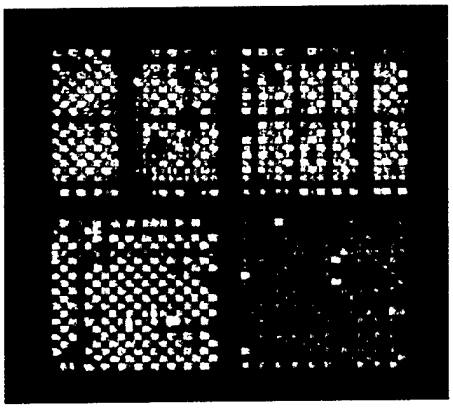

Figure 45: Checkerboard pattern displayed on all four arrays.

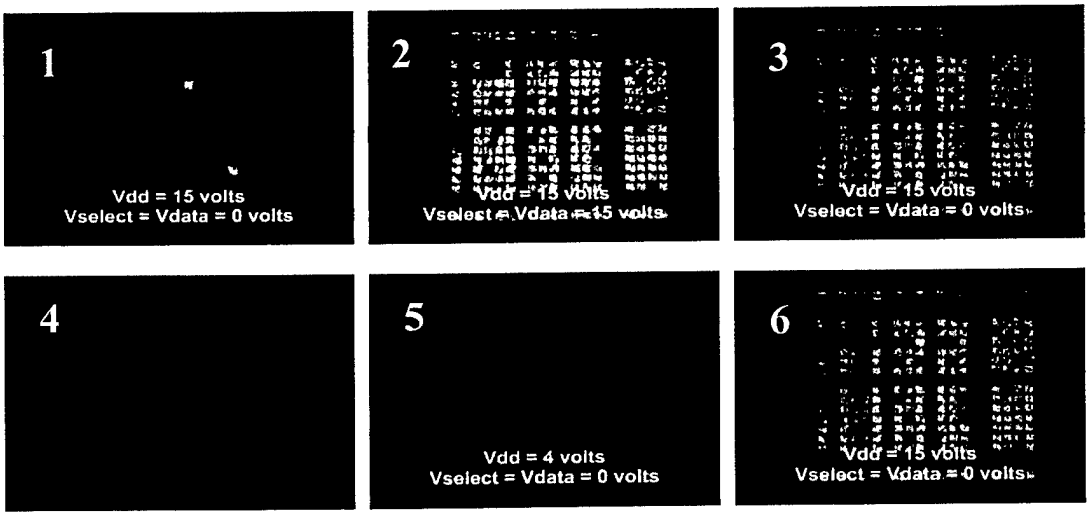

Figure 46: Testing of electrical feedback bi-stable array.

Figure 47: Laser spot swiped across optical feedback bi-stable pixel array in on-state.

Summary for Bi-stable a-Si TFTs

Arrays of bi-stable a-Si TFT phosphorescent OLED active matrix pixels were designed and fabricated using two different approaches, optical and electrical feedback. Arrays using both pixel designs were able to display images and the electrical feedback array showed excellent bi-stability. The electrical feedback pixels were able to retain image information indefinitely at low voltages/power (OLEDs turned off) while the the optical feedback pixels were found to be light sensitive and slowly (tens of seconds) turn off after being set to the on-state. The performance of the optical feedback bi-stable pixel most likely could be improved with minor modifications to the pixel design.

4. DISCUSSION

The objective of this program was to demonstrate a flexible, rugged, bright and efficient phosphorescent OLED technology with a low cost manufacturing path. The program focused on developing the technology to enable reliable low power consumption OLED displays to be fabricated on plastic substrates. This involved the integration of phosphorescent OLEDs (PHOLED™s) with multi-layer permeation barriers deposited both over the substrate and as a thin film encapsulant over the OLED to prevent degradation by oxygen or moisture. Additional tasks were development of large area, low cost organic vapor phase deposition (OVPD) fabrication technology, along with novel approaches to demonstrating bistable OLED pixels for advanced displays with reduced information bandwidth requirements.

4.1 Multi-layer Encapsulation Technology for Flexible OLED Displays

During the course of this program very good progress was made with regard to both barrier coated flexible substrates and monolithic encapsulation to enable reliable OLED devices to be fabricated on flexible plastic substrates. The multi-layer encapsulation technology developed by the Team led to the fabrication of OLEDs on plastic substrates with lifetimes of several thousand hours, in addition to providing for significant flexibility. Further work is still required to produce flexible displays with comparable lifetimes to those fabricated on glass substrates with conventional glass or metal can lids including dessicants. The flexible OLED display technology developed under this program is now being continued under funding from the Army Research Laboratory contract # DAAD19-02-2-0019. While alternative encapsulation approaches are being developed by other companies, we believe that the approach developed under this program will enable the manufacture of flexible OLED displays for both military and commercial applications.

The manufacture of OLED displays on flexible low cost substrates will also enable a shift in production technology from batch processing to roll to roll processing. While there will initially be many challenges in ensuring comparable yields from roll to roll manufacturing as from batch processing, once this has been accomplished, there will be significant potential cost savings. The production of flexible displays enables the realization of a new generation of mobile communication devices with light, thin form factor, high information content displays which can be rolled out when in use, and rolled away when not in operation. We believe that our phosphorescent OLED technology represents the most effective path to producing low power consumption flexible video-rate displays.

In addition to further basic flexible display development, the commercialization of flexible OLED displays will require the establishment of the necessary manufacturing infrastructure, and in particular the development of flexible active matrix backplanes.

4.2 Organic Vapor Phase Deposition (OVPD) of OLEDs

In the realm of manufacturing, we demonstrated that the new technology of organic vapor phase deposition (OVPD) first demonstrated by our team for use in the growth of nonlinear optical organic crystals, could also be adapted to the growth of OLEDs for large area displays. Hence, we demonstrated the growth of OLEDs employing this efficient manufacturing process with performance comparable to that of devices grown by vacuum deposition. A major innovation in OVPD growth under this program was the growth at reduced pressures – typically ~0.1-1 Torr – to obtain high density, high quality films. We have been able to demonstrate, based on conditions predicted in our models, the deposition of pixels with 6 micron diameters, and pattern resolutions approaching 1 micron. Our team is also working with Aixtron, AG, the largest supplier of MOCVD equipment worldwide. Aixtron, in partnership with Universal Display Corp. and Princeton University, is building both research and manufacturing OVPD tools for the display industry. OVPD has also proven its utility in the growth of high mobility pentacene organic thin film transistors. For example, we demonstrated that OVPD could be used under a variety of growth conditions to control the crystallite size of the organic in the channel of the transistor. Under appropriate, near equilibrium growth conditions, we obtained field effect mobilities of 1.4 cm^2/V-s with crystals extending across the entire several micron long gate region from source to drain. Such thin film transistors are of interest for fully organic display back planes, and their demonstration was a further objective of our program.

4.3 Bistable OLED Pixels

During this program we demonstrated two different approaches to enabling bistable OLED pixels. The shorter term path was based on using conventional amorphous silicon TFT technology to provide both the gain and optical sensors to achieve bistability. For a longer term, lower cost solution, we have demonstrated a novel integrated pixel using both OLEDs and organic photodetectors. Both strategies will be instrumental in the realization of new display architectures which can reduce both the power consumed in a display, and perhaps more importantly, the information bandwidth necessary to drive a display. In current flat panel displays, every pixel is updated at the display frame rate, usually around 60Hz, and this necessitates a large flow of data to the display, even if there is no change in the display image. In the future, as the information content of displays increases significantly, sending all the signal data to the array will become a major challenge. The fabrication of displays incorporating bistable pixels is a means to overcome the information bandwidth limitations.

Clearly for this technical approach to be commercialized, several system considerations need to be addressed. Firstly, one would like to enable grey scale display operation, as opposed to just binary operation. Secondly new driver chips would need to be available to take advantage of the display only needing to be updated whenever the information content is changed. We believe that the concepts developed in this program will be incorporated into future OLED displays as the reduction of information bandwidth in high information content displays enabled by the utilization of bistable pixels becomes more and more advantageous.

4.4 Commercialization Path

UDC's primary strategy is to broadly and non-exclusively license its technology. By so doing, UDC will strongly support broad technology diffusion. With the exclusive license rights to Princeton and USC's OLED technology and the acquisition of Motorola's OLED patent portfolio, UDC has the rights to over 450 issued and pending patents worldwide. For example, it recently announced partnerships with Sony Corporation, Samsung SDI, DuPont Displays, and Toyota Industries, and entered into strategic partnerships with Aixtron AG to co-develop UDC's organic vapor phase deposition (OVPD) technology, and with PPG Industries, Inc. to accelerate the development and supply of UDC's PHOLED materials. Today, this Team is recognized as one of the leading technology developers in this field with a well-qualified management team to broadly commercialize this technology.

This DARPA funded program has contributed to our technology base that UDC will license for manufacture of its proprietary OLED technologies.

5. CONCLUSIONS

This 30 month effort has resulted in many advances in the state of the art in OLED technology, and in some cases has set the agenda and standard for current and future research on OLEDs world wide. The technologies with the most profound impact are the demonstration of electrophosphorescent low power consumption OLEDs in flexible displays, thin film packaging for the reliable operation of flexible OLED displays, organic vapor phase deposition, and bistable OLED pixels. Several UDC commercialization partners have now demonstrated prototype displays based on UDC's proprietary phosphorescent OLED technology, including Samsung SDI and AU Optronics.

This program has also resulted in a strong collaboration between UDC, USC, Princeton University, Penn State University, Vitex Corporation and L3 Displays. Indeed, DARPA funds and AFRL management have played an important role in the success of this program, and the technology demonstrated through this program has significantly accelerated the commercialization of OLED technology for both consumer and military applications.

6. RECOMMENDATIONS

While enormous ground in OLED research and development has been covered under the auspices of this grant, and indeed by the entire technical community during the duration of this work, still much is left to be done if we are to realize the full potential of this strategically important device concept. Four major issues and challenges should be addressed in future work as described below.

6.1 Glass Substrate Products

The operational lifetime of OLEDs on-glass requires further improvements, particularly at high brightness and at elevated temperatures. This is particularly true of the blue phosphor and fluorescent family of dopants. Blue emission presents special challenges of both a fundamental and practical nature, which have yet to be fully understood. This remains a most fruitful area of research and development.

6.2 Manufacturing Technology/Ovpd

Low cost patterning and deposition of organic thin films over large substrate areas, and on flexible substrates has yet to be convincingly demonstrated. OLED technology is arguably the most powerful paradigm shift in display technology since the invention of the LCD. However, to displace LCDs, OLEDs must be capable of manufacture at very low cost and at high throughput and yields. Here, organic vapor phase deposition technology is of particular promise for the solution of these problems.

6.3 Flexible Substrate/Encapsulation Technology

Flexible, long operational lifetime displays fully integrated with advanced electronics promises to usher in a new generation of communication devices that are lightweight, compact, and highly portable. Yet, operational lifetime and fabrication issues that are still unsolved for OLEDs deposited on glass substrates are even more difficult to address for flexible displays on plastic substrates. However, the advantages brought by such integrated flexible displays make the challenges highly worthwhile to address and to solve.

6.4 Flexible Active Matrix Backplanes For Oled Displays

While passive matrix architectures can be successfully used to build OLED displays up to approximately 3" in size, or up to 200 line resolution, larger or higher information content displays require an active matrix drive. Both poly-Si and amorphous Si technologies are now looking promising as viable sources of OLED backplanes for rigid OLED displays. However, to date the development of flexible active matrix backplanes is still in its infancy, and the large scale production of these flexible TFT arrays is probably the major hurdle to the commercialization of flexible AMOLED displays.

7. SYMBOLS, ABBREVIATIONS, AND ACRONYMS

a-Si	Amorphous Silicon
AFRL	Air Force Research Laboratory (in Dayton OH)
Alq_3	Tris(8-hydroxyquinolinato) aluminum, aka aluminum trisquinolate, (electron transporting layer material; also, the emissive layer in original OLEDs)
AM	Active matrix (active element holds desired electrical signal for full frame time), (backplane substrate TFT array used to address AMOLED), (see passive matrix)
AMOLED	Active matrix organic light emitting display
Backplane	Electrical circuitry built on back substrate of a flat panel display to apply electrical representation of an image in a manner (driver-conditioned signals) that modulates/controls photonic emission from each picture element.
BAlq	Aluminum(III)bis(2-methyl-8-quinolinato)4-phenylphenolate, (hole blocking layer material)
BCP	2,9-dimethyl-4,7-diphenyl-1,10-phenanthroline (hole blocking layer material)
Brightness	Psychological dimension in which visual stimuli are ordered continuously from light to dark and which is correlated with light intensity
CBP	N,N'-dicarbazolyl-4,4'-biphenyl (host material for emissive layer of device)
Candella	Luminous intensity of a source emitting 540 GHz radiation at an intensity of 683^{-1} w sr^{-1} in a given direction.
Cd	Candella
cd/m^2	Candella per square meter (standard unit of luminous intensity per unit area)
cd/A	Candella per Ampere (unit for measuring of luminance efficiency) (unit of energy conversion efficiency in current driven device)
CIE	Commission Internationale de lÉclairage (standard color space coordinates)
cm^2/V-s	Unit of charge mobility (in semiconductor materials subjected to electric field)
CMOS	Complementary metal oxide semiconductor (power-conserving circuit design)
CRI	Color rendering index
CuPc	Copper phthalocyanine (hole injection layer material)
DARPA	Defense Advanced Research Projects Agency
DCM2	Red dye (a fluorescent material)
EBL	Electron blocking layer
EL	Electroluminescent
Electroluminescence	Luminescence resulting from application of electrical energy to a material
Electrophosphorescence	Luminescence caused by application of electrical power (current) via energy excited states similar to, or identical with, those involved in phosphorescence
EPR	Electron paramagnetic resonance.
ET	Electron transporter (layer within a device structure)
ETM	Electron transporter material
Fluorescence	Radiation emitted (usu. visible) resulting from and occurring only during the absorption of radiation (e.g. ultraviolet or two-photon infrared) from some other source. The absorbed radiation (e.g. UV) is often the result of an electrical

	discharge, with two energy conversions occur (from electrical to optical UV to visible).
Fluorescent	Glowing as a result of fluorescence
FOLED™	Flexible OLED
HBL	Hole blocking layer
HDS	High Definition Systems (applied research program for displays at DARPA)
HOMO	Highest occupied molecular orbital
HRL	Hughes Research Lab (in Malibu CA)
HT	Hole transporter (layer within a device structure)
HTM	Hole transporter material
IP	Intellectual property
Ir	Iridium (atomic element)
Ir complexes	Heavy metal complex dopant, or phosphor, based on Ir
$Ir(ppy)_3$	Iridium tris-(phenyl-pyridine). (Also sometimes written Irppy)
ISB	*bis*-iminostilbene-biphenyl
ITO	Indium tin oxide (material for fabrication of transparent, thin-film electrodes)
KOH	Potassium hydroxide (etching solution used in thin-film electronics fabrication)
L_o	Initial luminance (value at t = 0 for a newly made display device)
LE	Luminous efficiency (in cd/A)
lm	Lumen
lm/W	Lumen per Watt (power conversion efficiency unit for electro-optical device)
Lumen	Unit of luminous flux equal to the light emitted in a unit solid angle by a uniform point source of one candella intensity.
luminance	Luminous intensity of a surface in a given direction per unit of projected area
luminescence	Quality or state of emitting or reflecting usu. steady, suffused, or glowing light
lumophore	luminescent molecule
LX	ancillary bidentate (ligand)
LUMO	Lowest unoccupied molecular orbital
MOCVD	Metal oxide chemical vapor deposition
NPD	N,N'-diphenyl-N,N'dinapthylbenzidine (hole transporting material)
OLED	Organic light emitting diode (device, display)
OTS	octadecyltrichlorosilane
OVPD™	Organic vapor phase deposition
PHOLED™	Phosphorescent OLED
Phosphorescence	Luminance that is caused by the absorption of radiations and continues for a noticeable time after these radiations have stopped; an enduring luminescence without sensible heat. Emission is from an excited state with forbidden direct transition to ground state (i.e. low probability direct optical transitions), (e.g. triplet excited state emissions in most materials).
Phosphorescent	Light emitted involving non-optically allowed transitions
Pixel	Picture element, smallest portion of a display device capably of producing the full range of colors, graylevels, and angular distribution function of the full display

PM	Passive matrix (multiplexed electrical addressing scheme involving the sequential application of signals to each pixel of the display device; no active element exists in the display screen to retain the image control signals during frame time), (perception of a complete image relies on the relatively slow chemistry in the retina of the human eye to create an illusion that the entire image is present), (OLED light emission occurs only at moment control signal is applied to pixel). is present), (requires higher peak power or current at each pixel).
PMOS	Positively-doped-channel metal oxide semiconductor
POEM	Center for Photonics and Optoelectronic Materials (at Princeton University)
PU	Princeton University (in Princeton NJ)
Si	Silicon (atomic element)
SOLED	Stacked OLED
$T_{1/2}$	Half-life (in hrs)
TFT	Thin film transistor
TOLED™	Transparent OLED
Torr	Unit of pressure
UDC	Universal Display Corporation (in Ewing NJ)
USC	University of Southern California (in Los Angeles CA)
UV	Ultraviolet
VTE	Vacuum Thermal Evaporation
WOLED	White OLED
α-NPD	4,4'-bis[N-(1-naphthyl)-N-phenylamino]biphenyl (an HTL material)
η_{ext}	External quantum efficiency
λ_{max}	Wavelength at which maximum light emission is observed
Ω	Ohm

This page intentionally left blank.

APPENDIX A.

LIST OF TECHNICAL JOURNAL PUBLICATIONS RESULTING FROM THIS DARPA-SPONSORED AFRL-MANAGED CONTRACT

1. "Material Transport Regimes and Mechanisms for Growth of Molecular Organic Thin Films Using Low-Pressure Organic Vapor Phase Deposition", M. Shtein (Princeton, NJ), H. F. Gossenberger, J. B. Benziger and S. R. Forrest, J. Appl. Phys., **89**, 1470 (2001).
2. "Efficient Electrophosphorescence Using a Doped Ambipolar Conductive Molecular Organic Thin Film", C. Adachi, R. Kwong, and S. R. Forrest, Organic Electron., 2, 37 (2001).
3. "High Efficiency Red Electrophosphorescent Devices", C. Adachi, S. Lamansky, M. A. Baldo, R. Kwong, M. E. Thompson and S. R. Forrest, Appl. Phys. Lett., 78 1622 (2001).
4. "Lithium Doping of Semiconducting Organic Charge Transport Materials", G. Parthasarathy, C. Shen, A. Kahn and S. R. Forrest, J. Appl. Phys., 89, 4986 (2001).
5. "Highly Phosphorescent bis-Cyclomated Iridium Complexes: Synthesis, Photophysical Characterization and Use in Organic Light Emitting Diodes", S. Lamansky, P. Djurovich, D. Murphy, F. Abdel-Razzaq, H.-E. Lee, C. Adachi, P. E. Burrows, S. R. Forrest and M. E. Thompson, J. Am. Chem. Soc., 123, 4304 (2001).
6. "High efficiency yellow double-doped organic light emitting devices based on phosphor sensitized fluorescence", B. W. D'Andrade, M. A. Baldo, C. Adachi, J. Brooks, M. E. Thompson and S. R. Forrest, Appl. Phys. Lett., 79, 1045 (2001).
7. "Direct observation of structural changes in organic light emitting devices during degradation", D. Kolosov, D. S. English, V. Bulovic, P. F. Barbara, S. R. Forrest and M. E. Thompson, J. Appl. Phys., 90, 3242 (2001).
8. "Endothermic Energy Transfer: A Mechanism for Generating Very Efficient High Energy Phosphorescent Emission in Organic Materials", C. Adachi, R. C. Kwong, P. Djurovich, V. Adamovich, M. A. Baldo, M. E. Thompson, and S. R. Forrest, Appl. Phys. Lett., 79, 2082 (2001).
9. "Nearly 100% internal phosphorescence efficiency in an organic light emitting device", C. Adachi, M. A. Baldo, M. E. Thompson and S. R. Forrest, J. Appl. Phys., 90, 5048 (2001).
10. "Organic thin-film transistors based on bis(1,2,5 thiadiazolo)-p-quinobis(1,3-dithiole)", J. Xue and S. R. Forrest, Appl. Phys. Lett., 79, 3714 (2001).
11. "Nanolithography based on patterned metal transfer and its application to organic electronic devices", C. Kim, M. Shtein and S. R. Forrest, Appl. Phys. Lett., 80, 4051 (2002).
12. "Effects of film morphology and gate dielectric surface preparation on the electrical characteristics of organic vapor phase deposited pentacene thin-film transistors", M. Shtein, J. Mapel, J. B. Benziger, and S. R. Forrest, Appl. Phys. Lett., 81, 268 (2002).
13. "Electrophosphoresent p-i-n organic light emitting devices for very high efficiency flat panel displays", M. Pfeiffer, S. R. Forrest, K. Leo and M. E. Thompson, Adv. Mat., 14, 1633 (2002).
14. J. A. Nichols, T. N. Jackson, M. Lu, and M. Hack, "Bi-stable a-Si:H TFT Phosphorescent OLED

Active Matrix Pixel," 61st Device Research Conference Digest, (June 2003).

15. T. N. Jackson, "Thin Film Electronics for Active Matrix Flexible Displays," Flexible Displays & Electronics 2003, (March 2003).

16. J. A. Nichols, T. N. Jackson, M. Lu, and M. Hack, a-Si:H TFT Phosphorescent OLED Active Matrix Pixel," 2002 Society for Information Display Mid Atlantic Chapter OLED Research and Technology Conference Digest, (October 2002).

17. T. N. Jackson, "Flexible Substrate Active Matrix Display Backplanes," 2002 Society for Information Display Mid-Atlantic Conference Proceedings, (October 2002). Invited talk.

18. J. A. Nichols, M. Liu, M. Hack, and T. N. Jackson, "a-Si:H TFT Phosphorescent OLED Active Matrix Pixel," 2002 Society for Information Display Mid-Atlantic Conference Proceedings, p. 1368-1371, (October 2002).

19. T. N. Jackson, "Thin Film Electronics - Electronics Anywhere," Proceeding of the Imaging Science and Technology NIP18: International Conference on Digital Printing Technologies, p. 397-399 , San Diego (October 2002).

20. M. Hack, M. Lu, J.A. Nichols, R. Kwong, M. S. Weaver, and T. N. Jackson, "High Efficiency Phosphorescent OLEDs and their Addressing with Poly or Amorphous TFTs," Eurodisplay 2002 Proceedings, p. 21-24, (October 2002).

21. T. N. Jackson, "Organic Thin Film Electronics - Electronics Anywhere," 2002 SPIE Annual Meeting Digest, Conf. 4800, paper 66 (July 2002).

22. J. A. Nichols, T. N. Jackson, M. Lu, and M. Hack, "Phosphorescent OLED Amorphous Silicon TFT Active-Matrix Pixel," 44th Electronic Materials Conference Digest, June 2002).

23. J.A. Nichols, T.N. Jackson, M. Lu, and M. Hack, "a-Si:H TFT Active Matrix Phosphorescent OLED Pixel," 2002 Society for Information Display International Symposium Digest, 33, pp. 1368-1371, (May 2002).

24. M. Schwambera, N. Myer, S. Leder, M. Reinhold, M. Dauelslberg, G. Strauch, M. Heuken, H. Juergensen, T. Zhou, T. Ngo, and J. Brown, "Modeling and Fabrication of Organic Vapor Phase Deposition (OVPD) Equipment for OLED Display Manufacturing" 2002 Society for Information Display International Symposium Digest, 33, pp. 894-897, (May 2002).

25. P. E. Burrows, G. L. Graff, M. E. Gross, P. M. Martin, M. Hall, E. Mast, C, Bonham, W. Bennett, L. A. Michalski, M. S. Weaver, J. J. Brown, D. Fogarty, L. S. Sapochak, "Gas Permeation and Lifetime Tests On Polymer-Based Barrier Coatings", SPIE proc. 4105, "Organic Light-Emitting Materials and Devices IV" Editor(s): Kafafi, Z. H., 75-83 (2001).

26. M. S. Weaver, R. H. Hewitt, R. C. Kwong, S. Y. Mao, L. A. Michalski, T. Ngo, K. Rajan, M. A. Rothman, and J. A. Silvernail. W. D. Bennet, C. Bonham, P.E. Burrows, G. L. Graff, M.E. Gross, M. Hall, E. Mast and P. M. Martin, "Flexible Organic Light Emitting Devices", Proceedings of SPIE Vol 4295 "Flat Panel Display Technology and Display Metrology II" Editor(s): Kelley, E. F.; Voutsas, T. Published: April 2001

27. M. S. Weaver, J. J. Brown, R. H. Hewitt, S. Y. Mao, L. A. Michalski, T. Ngo, K. Rajan, M. A. Rothman, J. A. Silvernail, W. E. Bennet, C. Bonham, P. E. Burrows, G. L. Graff, M. E. Gross, M. Hall, E. Mast, and P. M. Martin, "Flexible Organic LEDs: Plastics Promise Thin Panels but Present New Problems Information Displays", SID publication, 17 5-6, 26-29 (2001).

28. M. Hack, M. S. Weaver, J. K. Mahon and J. J. Brown, "Recent Progress in Flexible OLED Displays", SPIE proc., Vol. **4362**, 245-254 (2001).

29. M. S. Weaver, A. B. Chwang, M. A. Rothman, J. A. Silvernail, M. G. Hack, J. J. Brown, P. E. Burrows, G. L. Graff, M. E. Gross, P. M. Martin, M. Hall, E. Mast, C. Bonham, W. Bennett and M. Zumhoff, "Recent progress in flexible displays", Cockpit Displays IX: Displays for Defense Applications SPIE proc., Editor. D. G. Hopper, Vol. 4712 237-249 (2002).

30. M. S. Weaver, L. A. Michalski, K. Rajan, M. A. Rothman, J. A. Silvernail, J. J. Brown, P. E. Burrows, G. L. Graff, M. E. Gross, P. M. Martin, M. Hall, E. Mast, C. Bonham, W. Bennett and M. Zumhoff."Organic light-emitting devices with extended operating lifetimes on plastic substrates", Appl. Phys. Lett., 81, 2929-2931 (2002).

31. A. B. Chwang, M. A. Rothman, S. Y. Mao, R. H. Hewitt, M. S. Weaver, J. A. Silvernail, K. Rajan, M. Hack, J. J. Brown, X. Chu, L. Moro, T. Krajewski and N. Rutherford, "Thin film encapsulated flexible OLEDs", Proceedings of *the Society for Information Display, Digest of Technical Papers*, vol. 34, no. 2, pp. 868-871, 2003.

This page intentionally left blank.

APPENDIX B.

LIST OF ADVANCED DEGREES AWARDED FOR RESEARCH ACCOMPLISHED UNDER THIS DARPA-SPONSORED CONTRACT

Advanced degrees awarded in association with research sponsored under this grant are listed below by institution in the following format: (date, recipient, type of degree, thesis title).

Princeton University:

None

University of Southern California:

Dmitry Kolosov: Ph.D. 2001
"Part 1: 1,8-Naphtylamides as Novel Materials for Phosphorescent Organic Light Emitting Devices and Degradation Studies of Transparent Light Emitting Devices, Part 2: Reaction Dynamics of C(3P) with Chloroform"

Douglas Loy: Ph.D. 2000
"Molecular Hole Transporting materials for Organic Light Emitting Diodes"

Sergey Lamansky: Ph.D. 2001
"Chemistry of Novel Iridium and Platinum orhto-Metallated Complexes and Decaarylplumbacenes for Organic Light Emitting Diodes"